Lipid hydroperoxides promote muscle atrophy through lysosomal amplification

Hiroaki Eshima,[1-3] Piyarat Siripoksup,[1,4] Justin L. Shahtout,[1,4] MacKenzie J. Pearson,[5] Ziad S. Mahmassani,[1,2,4] Patrick J. Ferrara,[1,2,6] Alexis W. Lyons,[1] J. Alan Maschek,[1,6,7] Alek D. Peterlin,[1,6] Anthony R. P. Verkerke,[1,6] Jordan M. Johnson,[1,6] Anahy Salcedo,[1] Jonathan J. Petrocelli,[1,4] Ethan J. Anderson,[8] Sihem Boudina,[1,2,6] Qitao Ran,[9] James E. Cox,[1,7,10] Micah J. Drummond,[1,2,4] Katsuhiko Funai,[1,2,4,6]*

[1]Diabetes & Metabolism Research Center, University of Utah, Salt Lake City, Utah, USA

[2]Molecular Medicine Program, University of Utah, Salt Lake City, Utah, USA

[3]Department of International Tourism, Nagasaki International University, Sasebo, Nagasaki, Japan

[4]Department of Physical Therapy & Athletic Training, University of Utah, Salt Lake City, Utah, USA

[5]Sciex, Framingham, MA, USA

[6]Department of Nutrition & Integrative Physiology, University of Utah, Salt Lake City, Utah, USA

[7]Metabolomics Core Research Facility, University of Utah, Salt Lake City, Utah, USA

[8]Fraternal Order of Eagles Diabetes Research Center, University of Iowa, Iowa City, Iowa, USA

[9]Department of Cell Systems and Anatomy, University of Texas Health Science Center at San Antonio, San Antonio, Texas, USA

[10]Department of Biochemistry, University of Utah, Salt Lake City, Utah, USA

*Corresponding Author:

Katsuhiko Funai, Ph.D.

Diabetes & Metabolism Research Center

28 15 N 2030 E, Salt Lake City, UT 84112

29 Phone: (801) 585-1781

30 Fax: (801) 585-0701

31 Email: kfunai@health.utah.edu

Abstract

Reactive oxygen species (ROS) is a cardinal feature of skeletal muscle atrophy. However, ROS refers to a collection of radical molecules whose cellular signals are vast, and it is unclear which downstream consequences of ROS are responsible for the loss of muscle mass and strength.[1,2] Here we show that lipid hydroperoxides (LOOH) are increased with age and disuse, and the accumulation of LOOH by suppression of glutathione peroxidase 4 (GPx4) is sufficient to augment muscle atrophy. Strikingly, genetic and pharmacologic suppression of muscle LOOH robustly prevented the reduction of both muscle mass and force-generating capacity. LOOH promoted atrophy in a lysosomal-dependent, proteasomal-independent manner, and the suppression of autophagic machinery was sufficient to prevent muscle atrophy and weakness. Indeed, the lysosome is essential for the amplification of LOOH induced by oxidative stress. Our findings provide novel insights for the role of LOOH in muscle atrophy including a therapeutic implication by pharmacologic suppression.

Main

Loss of muscle mass and function with age is detrimental to health and quality of life.[3,4] A pharmacologic therapy for muscle loss does not exist, and current diet or exercise therapeutic approaches are often ineffective or unfeasible. Oxidative stress has been implicated in muscle atrophy by accelerating proteolysis,[2] but the exact mechanism by which ROS contributes to the decrease in muscle mass and strength is not well understood. Lipid hydroperoxide (LOOH) is a class of lipid ROS molecules that has been implicated in cell damage, particularly as a trigger to induce ferroptosis, a non-apoptotic form of regulated cell death.[5,6] LOOH propagation is endogenously suppressed by GPx4 that catalyzes the reaction by which LOOH is reduced to its nonreactive hydroxyl metabolite.[7] However, the role of LOOH in skeletal muscle is not well understood.[8,9]

58 We first evaluated the changes in skeletal muscle LOOH with aging. In humans and
59 in mice, aging promoted a reduction in the expression of GPx4 in skeletal muscle (Fig.
60 1a&b). To examine the changes in skeletal muscle LOOH landscape with age, we
61 performed a comprehensive oxidolipidomic analysis in muscle samples from young (4
62 months) and old (20 months) mice (Fig. 1c&d). We detected over 300 species of oxidized
63 lipids with an effect distribution that was highly class-dependent. Among these, age had the
64 most robust effect on oxidized phosphatidylethanolamine (Fig. 1c, red), a class of lipids that
65 have been implicated as a potential lipid signal to induce ferroptosis.[10] Among the top ten
66 oxidized lipid species whose abundance was most robustly increased with age, six of them
67 were oxidized phosphatidylethanolamine (Figure 1d), and they were substantially more
68 highly abundant compared to other oxidized lipids. LOOH can be indirectly assessed by
69 quantifying LOOH adducts such as 4-hydroxynonenal (4-HNE) and malondialdehyde
70 (MDA). We confirmed increased muscle 4-HNE and MDA with age (Extended Data Fig. 1a-
71 c).
72 Disuse also promotes skeletal muscle atrophy that is likely contributed by ROS.[2] To
73 model disuse atrophy, mice underwent a hindlimb unloading (HU) procedure as previously
74 described.[11,12] As expected, HU induced muscle atrophy and weakness (Fig. 1e&f)
75 concomitant to reduction in body and lean mass (Extended Data Fig. 1d-f). Disuse robustly
76 elevated muscle LOOH levels (Fig. 1g, Extended Data Fig. 1g) without significant changes
77 in mitochondrial bioenergetics (Extended Data Fig. 1h-j). An increase in muscle LOOH
78 preceded atrophy, consistent with the notion that LOOH may trigger mechanisms to
79 promote loss of muscle mass.
80 Next, we tested our hypothesis that LOOH contributes to muscle atrophy using
81 C2C12 myotubes (Fig. 1h). Lentivirus-mediated knockdown (KD) of GPx4 increased LOOH
82 and markers of ferroptosis (Extended Data Fig. 2a-f) concomitant with a decrease in
83 myotube diameter (Fig. 1i&j). We also recapitulated these findings with erastin (system X_c^-
84 inhibitor that suppresses glutathione synthesis) (Fig. 1i&j and Extended Data Fig. 2g-k) and

85 RSL3 (GPx4 inhibitor) (Fig. 1i&j and Extended Data Fig. 2l-o), commonly used acute
86 pharmacological interventions to elevate intracellular LOOH. We then translated these
87 findings in vivo with global heterozygous GPx4 knockout mice ($GPx4^{+/-}$). Germline deletion
88 of GPx4 is embryonically lethal,[13] but $GPx4^{+/-}$ mice appear normal and do not have an
89 observable muscle phenotype at baseline.[7,14] We studied 4 months (young) and 20 months
90 (old) $GPx4^{+/-}$ and wildtype littermates with or without HU (Extended Data Fig. 3a-d). In
91 young mice, GPx4 haploinsufficiency augmented the loss in muscle mass induced by HU
92 (Fig. 2a and Extended Data Fig. 3e). However, muscle masses between old $GPx4^{+/-}$ and
93 wildtype mice were not different. We interpret these findings to mean that disuse in old
94 mice promotes an increase in LOOH that has already reached a maximally effective
95 threshold with age such that GPx4 deletion had no further effect. In support of this, we saw
96 no differences in 4-HNE or MDA levels between old $GPx4^{+/-}$ and wildtype mice (Fig. 2b and
97 Extended Data Fig. 3f&g). GPx4 haploinsufficiency did not alter force-generating capacity
98 (Fig. 2c and Extended Data Fig. 3h-j).
99 Because GPx4 is expressed globally, we also studied mice with skeletal muscle-
100 specific tamoxifen-inducible GPx4 knockout (GPx4-MKO) (Fig. 2d and Extended Fig. 4a).[15]
101 Consistent with GPx4+/- mice, GPx4-MKO mice were also more prone to developing
102 disuse-induced skeletal muscle atrophy (Fig. 2e&f and Extended Data Fig. 4b-f)
103 concomitant to elevated LOOH (Fig. 2g and Extended Data Fig. 4g&h), suggesting that loss
104 of GPx4 in muscle augments atrophy in a cell-autonomous manner. Histological analyses
105 revealed that reduced muscle mass was consistent with reduced cross-sectional area of
106 myofibers regardless of fiber-type compositions (Fig. 2h&i and Extended Data Fig. 4i&j).
107 These data implicate that LOOH directly reduces muscle cell size in vivo.
108 GPx4 primarily neutralizes LOOH but it also exhibits some activity towards other
109 peroxides.[16] To confirm that the effects of GPx4 deletion to promote atrophy is specific to
110 LOOH, we diminished the ability of cells to incorporate polyunsaturated fatty acids (PUFAs)
111 into phospholipids by deleting lysophosphatidylcholine acyltransferase 3 (LPCAT3).[17-19]

112 LPCAT3 is an enzyme of Lands cycle that preferentially acylates lysophospholipids with
113 PUFAs, and thus an essential component of ferroptosis[10]. Indeed, LPCAT3 KD rescued the
114 increase in 4-HNE induced by GPx4 KD (Fig. 2j and Extended Data Fig. 5a-c).
115 Remarkably, deletion of LPCAT3 KD completely restored the reduction in myotube
116 diameter induced by GPx4 KD (Fig. 2k&l). Similarly, LPCAT3 deletion also prevented
117 LOOH and cell death induced by erastin (Extended Data Fig. 5d-h). These findings indicate
118 that muscle atrophy induced by loss of GPx4 or erastin treatment is due to the
119 accumulation of LOOH and not other peroxides.

120 Would suppression of LOOH be sufficient to ameliorate skeletal muscle atrophy? We
121 studied young (4 months) and old (20 months) global GPx4-overexpressing (GPx4Tg)
122 mice[20] with or without HU (Extended Data Fig. 6a-e). Strikingly, both young and old
123 GPx4Tg mice were resistant to disuse-induced muscle atrophy (Fig. 3a and Extended Data
124 Fig. 6f&g). Perhaps even more impactful was the effect of GPx4 overexpression on skeletal
125 muscle force-generating capacity such that, in both young and old, GPx4 overexpression
126 robustly protected mice from muscle weakness induced by HU (Fig. 3b and Extended Data
127 Fig. 6h-j). These findings are in contrast to our experiments in $GPx4^{+/-}$ mice where muscle
128 mass phenotype was only present in the young mice (Fig. 2a) and no phenotype on muscle
129 strength (Fig. 2b). Consistent with the notion that GPx4 overexpression acts on LOOH, HU-
130 induced increase in 4-HNE was completely suppressed in GPx4Tg mice (Fig. 3c and
131 Extended Data Fig. 6k). We also found that the protection from muscle atrophy was
132 explained by greater myofiber cross-sectional area regardless of fiber-type (Fig. 3d&e and
133 Extended Data Fig. 6l&m).

134 Next, we explored opportunities to pharmacologically suppress LOOH to prevent
135 muscle atrophy. Ferrostatin-1 is an inhibitor of ferroptosis that is widely used to study
136 LOOH.[21,22] Indeed, incubation of cells with ferrostatin-1 was sufficient to suppress LOOH
137 induced by GPx4 KD (Fig. 3f and Extended Data Fig. 7a) concomitant with protection from
138 myotube atrophy (Fig. 3g&h and Extended Data Fig. 7b&c). Nevertheless, ferrostatin-1 is

139 currently not an FDA approved drug with questions surrounding safety. Thus, we tested L-
140 carnosine, a dipeptide composed of beta-alanine and L-histidine that has the ability to
141 scavenge LOOH.[23,24] Similar to ferrostatin-1, L-carnosine was sufficient to rescue LOOH
142 and cell death induced by GPx4 KD (Extended Data Fig. 7d-f) or erastin (Extended Data
143 Fig. 7g-i). Leveraging these data, we performed a preclinical trial for L-carnosine provided
144 in drinking water ad lib (80 mM) in young wildtype C57BL6/J mice. L-carnosine treatment
145 did not alter body mass, body composition, food intake, and water intake (Extended Data
146 Fig. 7j-m), and successfully suppressed muscle LOOH induced by HU (Extended Data Fig.
147 7n&o). Remarkably, mice provided with L-carnosine were partly protected from disuse-
148 induced muscle atrophy (Extended Data Fig. 7p).
149 In humans, L-carnosine is rapidly degraded by a circulating carnosinase[25] that may
150 render oral carnosine treatment ineffective. In contrast, N-acetylcarnosine has a longer
151 half-life and may be a more effective reagent in humans thus improving its translational
152 potential. Similar to ferrostatin-1 and L-carnosine, N-acetylcarnosine also prevented LOOH
153 and cell death induced by GPx4 KD (Extended Data Fig. 8a-c) or erastin (Extended Data
154 Fig. 8d-f). Leveraging these findings, we proceeded with a preclinical trial for N-
155 acetylcarnosine in drinking water (80 mM, Fig. 3i) in young (4 months, C57BL6/J; Jax
156 colony) and old (20 months, C57BL/6; NIA rodent colony) wildtype mice. Similar to L-
157 carnosine treatment, N-acetylcarnosine did not alter body mass, body composition, food
158 intake, or water intake (Extended Data Fig. 8g-k), and successfully suppressed muscle
159 LOOH (Fig. 3j and Extended Data Fig. 8l&m). Strikingly, similar to our findings in GPx4Tg
160 mice, N-acetylcarnosine ameliorated muscle atrophy (Fig. 3k and Extended Data Fig. 8n)
161 and weakness (Fig. 3l and Extended Data Fig. 8o-q) in both young and old mice. Protection
162 from muscle atrophy was similarly explained by greater myofiber cross-sectional area
163 regardless of fiber-type (Fig. 3m&n and Extended Data Fig. 8r&s). These promising
164 observations inform a potential clinical trial to test the efficacy of N-acetylcarnosine
165 treatment in ameliorating muscle atrophy in humans.

166 What is the mechanism by which LOOH promotes muscle atrophy? C2C12 myotubes
167 were pretreated with Bafilomycin A1 (BafA1) or MG132 prior to erastin incubation to
168 determine whether LOOH increases protein degradation in a lysosomal- or proteasomal-
169 dependent manner, respectively. Erastin-induced reduction in myotube diameter was
170 suppressed with BafA1, but not with MG132 (Fig. 4a&b and Extended Data Fig. 9a),
171 suggesting that the lysosome mediates protein degradation by LOOH.[26] We also
172 reproduced these findings with RSL3 treatment (Extended Data Fig. 9b&c). How does
173 LOOH, a lipid molecule, promote lysosomal-degradation? Upstream of the lysosome,
174 autophagosome formation is mediated by a lipidation of LC3 by ATG3.[27] Thus, we
175 hypothesized that LOOH may affect the lipidation of LC3. Indeed, GPx4 KD drastically
176 reduced the protein content of p62, LC3-I and LC3-II (Fig. 4c and Extended Data Fig. 9d-h),
177 potentially suggesting that LOOH may accelerate lysosomal degradation by affecting LC3
178 lipidation. To test this possibility, we performed a targeted deletion of ATG3 in vitro. Indeed,
179 ATG3 KD completely rescued the reduction in myotube diameter induced by GPx4 KD (Fig.
180 4d&e and Extended Data Fig. 9i-l). Leveraging these findings, we generated mice with
181 skeletal muscle-specific tamoxifen-inducible ATG3 knockout (ATG3-MKO) (Fig. 4f and
182 Extended Data Fig. 10a-c) and studied them with or without HU (Extended Data Fig. 10d-f).
183 Loss of muscle ATG3 was protective from disuse-induced atrophy (Fig. 4g and Extended
184 Data Fig. 10g) and weakness (Fig. 4h and Extended Data Fig. 10h) which can be explained
185 by greater myofiber cross-sectional area (Fig. 4i&j and Extended Data Fig. 10i).
186 We initially hypothesized that lysosomal-degradation mediates LOOH-induced
187 protein degradation to contribute to muscle atrophy. However, further assessment of
188 muscle LOOH illuminated a more complex interaction between the lysosome and
189 LOOH.[28,29] Unexpectedly, quantification of 4-HNE revealed that inhibition of the autophagy-
190 lysosome axis by ATG3 deletion or BafA1 was sufficient to inhibit LOOH induced by GPx4
191 deletion, erastin, or RSL3 (Fig. 4k and Extended Data Fig. 10j-p). These findings suggest
192 that the autophagy-lysosome axis is essential for LOOH amplification, in addition to its

193 potential role in mediating protein degradation downstream. Indeed, immunofluorescence
194 experiments revealed that 4-HNE is highly co-localized to LAMP2 (Fig. 4l and Extended
195 Data Fig. 10q), consistent with the notion that the lysosome is necessary for LOOH
196 propagation. To support this idea, an increase in LOOH by hydrogen peroxide or
197 carmustine (agents that increase pan oxidative stress without acting on GPx4 directly) was
198 completely inhibited by lysosomal inhibition (Fig. 4n and Extended Fig. 10r-t). Together,
199 these observations suggests that the propagation of LOOH may be mediated by the
200 lysosome (Fig. 4o).

201 In summary, the current findings demonstrate a novel mechanism that indicate LOOH
202 as the key downstream molecule by which oxidative stress promotes muscle atrophy and
203 weakness. Skeletal muscle LOOH was robustly upregulated with aging and/or disuse, and
204 genetic or pharmacologic suppression of LOOH was sufficient to rescue muscle atrophy. In
205 particular, N-acetylcarnosine treatment shows a potent effect in preserving muscle mass
206 and strength with disuse in both young and old mice, informing the potential trial to utilize
207 this compound to ameliorate loss of muscle function in humans. We further provide
208 evidence that the autophagy-lysosome axis is essential for the propagation of LOOH,
209 suggesting a novel interaction between these cellular processes that could be interrogated
210 to ameliorate LOOH-induced damage.

211 **Methods**

212 **Animal models.** GPx4+/- and GPx4Tg mice were generated previously.[13,20] Conditional
213 GPx4 knockout (GPx4cKO+/+) mice were acquired from Jackson Laboratory (Stock No:
214 027964).[15] Conditional ATG3 knockout (ATG3cKO+/+) mice were previously described.[30]
215 GPx4cKO+/+ mice or ATG3cKO+/+ mice were then crossed with tamoxifen-inducible,
216 skeletal muscle–specific Cre recombinase (HSA-MerCreMer+/-) mice[31] to generate
217 GPx4cKO+/+; HSAMerCreMer-/- (control) and GPx4cKO+/+; HSA-MerCreMer+/- (skeletal
218 muscle–specific GPx4 knockout; GPx4-MKO) mice or ATG3cKO+/+; HSAMerCreMer-/-
219 (control) and ATG3cKO+/+; HSA-MerCreMer+/- (ATG3-MKO) mice. Tamoxifen-injected (7.5
220 µg/g body mass, 5 consecutive days) littermates were used. Mice were maintained on a 12-
221 hour light/12-hour dark cycle in a temperature-controlled room. Body composition
222 measurements were taken immediately before terminal experiments with a Bruker Minispec
223 MQ20 nuclear magnetic resonance (NMR) analyzer (Bruker, Rheinstetten, Germany). All
224 mice were bred onto C57BL/6J background and were born at normal Mendelian ratios. Body
225 mass were measured every day during HU. All protocols were approved by Institutional
226 Animal Care and Use Committees at the University of Utah.

227 **Hindlimb unloading.** Mice underwent 1, 7, or 14 days of HU (2 mice/cage) using a
228 previously described protocol[11,12] based on the traditional Morey-Holton design to study
229 disuse atrophy in rodents. Along with daily monitoring of body mass, food intake was
230 monitored every other day to ensure that the mice did not experience excessive weight loss
231 due to malnutrition or dehydration. Following 1, 7, or 14 days of HU, mice were fasted for 4
232 h and given an intraperitoneal injection of 80 mg/kg ketamine and 10 mg/kg xylazine, after
233 which tissues were harvested. Extensor digitorum longus (EDL), and soleus (SOL) were
234 carefully dissected for weight measurements.

235 **Muscle force generation.** Force-generating properties of soleus and EDL muscles were
236 measured as previously described.[32,33] Briefly, soleus/EDL muscles were sutured at each
237 tendon, and muscles were suspended at optimal length (Lo), which was determined by pulse
238 stimulation. After Lo was identified, muscles were stimulated (0.35 seconds, pulse width 0.2
239 milliseconds) at frequencies ranging from 10 to 200 Hz. Muscle length and mass were
240 measured to quantify cross-sectional area for force normalization.

241 **Quantitative reverse transcription PCR.** Samples were homogenized in TRIzol reagent
242 (Life Technologies) to extract total RNA. One microgram RNA was reverse-transcribed using
243 an IScript cDNA synthesis kit (Bio-Rad). Reverse transcription PCR (RT-PCR) was
244 performed with the Viia 7 Real-Time PCR System (Life Technologies) using SYBR Green

245 reagent (Life Technologies). All data were normalized to ribosomal L32 gene expression and
246 were normalized to the mean of the control group. Primers were based on sequences in
247 public databases.

248 **Western blot.** Whole muscle or cells were homogenized, and western blots were performed
249 as previously described.[11] Protein homogenates were analyzed for abundance of
250 phosphorylated 4-hydroxynonenal (4-HNE; ab48506; Abcam), GPx4 (ab125066, Abcam),
251 actin (A2066, MilliporeSigma), GAPDH (14C10, Cell Signaling Technology), p62 (ab56416,
252 Abcam), LC3B (83506, Cell Signaling Technology).

253 **Mass spectrometry.** Oxidolipidomics samples were analyzed on the SCIEX 7500 system
254 coupled with ExionLC (SCIEX, Concord, Canada) using multiple reaction monitoring (MRM)
255 analysis. Mobile phase A is composed of 93:7 acetonitrile:dichloromethane containing 2mM
256 ammonium acetate and mobile phase B is composed of 50:50 acetonitrile:water containing
257 2mM ammonium acetate. A Phenomenex Luna® NH2 3 µm particle size (4.6x150mm) was
258 used for separation and column temperature was kept at 40°C. The total flow rate is 0.7
259 mL/min with a total run time of 17-minutes. Samples were extracted using the Bligh & Dyer
260 method. Lower layer was collected, dried down and resuspended in mobile phase A.

261 **Cell culture.** C2C12 myoblasts were grown and maintained in high-glucose Dulbecco's
262 modified Eagle's medium (DMEM), with 10% fetal bovine serum (FBS), and 0.1 %
263 penicillin/streptomycin. Once 90 to 100% confluent, C2C12 cells were differentiated into
264 myotubes with low-glucose DMEM, with l-glutamine and 110 mg/L sodium pyruvate;
265 supplemented with 2% horse serum, and 0.1% penicillin-streptomycin. For experiments with
266 erastin (E7781, MilliporeSigma), Ferrostatin-1 (SML0583, MilliporeSigma), and RSL3
267 (SML2234, MilliporeSigma), C2C12 myotubes were incubated with either 10 µM erastin/10
268 µM Ferrostatin-1/5 µM RSL3/ or equal-volume DMSO directly dissolved into medium. For
269 experiments with L-carnosine (C9625, MilliporeSigma), and N-acetylcarnosine (18817,
270 Cayman), C2C12 myotubes were incubated with 10 mM of L-carnosine/N-acetylcarnosine
271 directly dissolved into medium.

272 **Lentivirus-mediated knockdown of GPx4/LPCAT3/ATG3** Lentivirus-mediated knockdown
273 of experiments were performed as previously described.[12,18,34] Vectors were decreased using
274 pLKO.1 lentiviral-RNAi system. Plasmids encoding short hairpin RNA (shRNA) for mouse
275 GPx4 (shGPx4: TRCN0000076552), mouse LPCAT3 (shLPCAT3: TRCN0000121437), and
276 mouse ATG3 (shATG3: TRCN0000247442) were obtained from MilliporeSigma. Packaging
277 vector psPAX2 (ID 12260), envelope vector pMD2.G (ID 12259), and scrambled shRNA
278 plasmid (SC: ID 1864) were obtained from Addgene. HEK293T cells in 10 cm dishes were

279 transfected using 50 μL 0.1% polyethylenimine, 200 μL 0.15 M sodium chloride, and 500 μL
280 Opti-MEM (with HEPES, 2.4 g/L sodium bicarbonate, and l-glutamine; Gibco 31985) with
281 2.66 μg of psPAX2, 0.75 μg of pMD2.G, and 3 μg of either scrambled or GPx4/LPCAT3/ATG3
282 shRNA plasmids. After 48 hours, growth medium was collected, filtered using 0.22 μm
283 vacuum filters, and used to treat undifferentiated C2C12 cells for 48 hours. To ensure that
284 only cells infected with shRNA vectors were viable, cells were selected with puromycin
285 throughout differentiation.

286 **Measurements of myotube diameter.** Images of myotubes were visualized at ×20
287 magnification using an inverted light microscope and captured with a camera (DP74,
288 Olympus). Myotube diameter was measured for at least 100 myotubes from 5 random fields
289 in each group using ImageJ software. The average diameter per myotube was calculated as
290 the mean of ten short-axis measurements taken along the length of the myotube.

291 **Assessment of cell death.** Cell death levels were examined by counting the numbers of
292 cells with trypan blue staining. The cells were trypsinized and stained with 0.2% trypan blue
293 for 5 min. Stained and non-stained cells were counted under a microscope using a
294 hemocytometer.

295 **Immunofluorescence.** C2C12 myotubes were fixed with 4% paraformaldehyde for 10 min
296 and permeabilized with 0.2% Triton X-100 for 15 min. After blocking with bovine serum
297 albumin, immunocytochemistry was performed with anti-HNE (ab48506, Abcam), anti-
298 lysosome associated membrane protein 2 (Lamp-2) (NB300-591, Novus), and Alexa Fluor-
299 conjugated secondary antibodies Alexa Fluor® 568 (ab175472, abcam), Alexa Fluor® 488
300 (ab150073, abcam), and DAPI (D1306, Invitrogen). Images were captured using a 63× 1.4
301 NA oil immersion objective on a Leica SP5 confocal system (Leica). For an experiment,
302 C2C12 myotubes incubated with erastin with or without pretreatment of BaFA1 (SML1661,
303 MilliporeSigma). Soleus muscles were embedded in optimal cutting temperature (OCT) gel
304 and sectioned at 10 μm with a cryostat (Microtome Plus). The sections underwent blocking
305 for 1 hr with M.O.M. mouse IgG Blocking Reagent (Vector Laboratories, MKB-2213), 1 hr
306 with primary antibodies (BA.D5, SC.71, BF.F3 all at 1:100 from DSHB). Sections were then
307 probed with the following secondary antibodies: Alexa Fluor 647 (1:250; Invitrogen, A21242),
308 Alexa Fluor 488 (1:500; Invitrogen, A21121), and Alexa Fluor 555 (1:500; Invitrogen, A21426).
309 Negative stained fibers were considered to be IIx. Slides were imaged with an automated
310 wide-field light microscope (Nikon Corp.) using a 10x objective lens. Cross-sectional area
311 and fiber type composition was then quantified utilizing ImageJ software.

312 **Mitochondrial respiration measurements.** Mitochondrial O_2 utilization was measured

313 using the Oroboros O_2K Oxygraphs, as previously described.[11,12] Isolated mitochondria were
314 added to the oxygraph chambers containing buffer Z. Respiration was measured in response
315 to the following substrate concentrations: 0.5 mM malate, 5 mM pyruvate, 2 mM ADP, 10 mM
316 succinate, and 1.5 μM FCCP.

317 **Mitochondrial H_2O_2 measurements.** Mitochondrial H_2O_2 production was measured using
318 the Horiba Fluoromax-4, as previously described.[11,12] Briefly, skeletal muscle was minced in
319 mitochondria isolation medium (300 mM sucrose, 10 mM HEPES, 1 mM EGTA) and
320 subsequently homogenized using a Teflon glass system. Homogenates were then
321 centrifuged at 800 g for 10 min, after which the supernatant was taken and centrifuged at
322 12,000 g for 10 min. The resulting pellet was carefully resuspended in mitochondria isolation
323 medium. JH_2O_2 was measured in buffer Z (MES potassium salt; 105 mM, KCl 30 mM,
324 KH_2PO_4 10 mM, $MgCl_2$ 5 mM, and BSA 0.5 mg/ml) supplemented with 10 μM Amplex
325 UltraRed (Invitrogen) and 20 U/mL CuZnSOD in the presence of the following substrates: 10
326 mM succinate, 100 μM 1,3-bis(2-chloroethyl)-1-nitrosourea (BCNU/carmustine), and 1 μM
327 auranofin. The appearance of the fluorescent product was measured with excitation/emission
328 at 565/600 nm.

329 **Administration of L-carnosine/N-acetylcarnosine in vivo.** Carnosine was administered
330 as previously described (75). Briefly, young (4-month-old) or old (20-month-old) C57BL/6J
331 mice were supplemented with 80 mM carnosine dissolved in drinking water (pH 7.5) for 2
332 weeks (1 week of pretreatment and 1 week during HU). Bottles were refreshed two times a
333 week (L-carnosine, C9625, MilliporeSigma), and or everyday (N-acetyl carnosine, 18817,
334 Cayman).

335 **MDA quantification.** MDA content was quantified in fresh gastrocnemius muscles using a
336 lipid peroxidation assay kit (ab118970, Abcam) according to the manufacturer's instruction.
337 Rates of appearance of MDA-thiobarbituric acid adduct were quantified colorimetrically at
338 532 nm using a spectrophotometer.

339 **Statistical analyses.** Data are presented as means ± s.e.m. Statistical analyses were
340 performed using GraphPad Prism 7.03. Independent sample t-tests (two-sided) were used
341 to compare two groups. For multiple comparisons, one- or two-way analysis of variance
342 (ANOVA) were performed followed by appropriate post-hoc tests corrected for multiple
343 comparisons. For all tests $P < 0.05$ was considered statistically significant.

344 **References**

345 1 Scicchitano, B. M., Pelosi, L., Sica, G. & Musaro, A. The physiopathologic role of
346 oxidative stress in skeletal muscle. *Mech Ageing Dev* **170**, 37-44,
347 doi:10.1016/j.mad.2017.08.009 (2018).
348 2 Powers, S. K., Smuder, A. J. & Criswell, D. S. Mechanistic links between oxidative
349 stress and disuse muscle atrophy. *Antioxid Redox Signal* **15**, 2519-2528,
350 doi:10.1089/ars.2011.3973 (2011).
351 3 Evans, W. J. Skeletal muscle loss: cachexia, sarcopenia, and inactivity. *Am J Clin*
352 *Nutr* **91**, 1123S-1127S, doi:10.3945/ajcn.2010.28608A (2010).
353 4 Larsson, L. *et al.* Sarcopenia: Aging-Related Loss of Muscle Mass and Function.
354 *Physiol Rev* **99**, 427-511, doi:10.1152/physrev.00061.2017 (2019).
355 5 Wiernicki, B. *et al.* Excessive phospholipid peroxidation distinguishes ferroptosis
356 from other cell death modes including pyroptosis. *Cell Death Dis* **11**, 922,
357 doi:10.1038/s41419-020-03118-0 (2020).
358 6 Yang, W. S. *et al.* Regulation of ferroptotic cancer cell death by GPX4. *Cell* **156**,
359 317-331, doi:10.1016/j.cell.2013.12.010 (2014).
360 7 Anderson, E. J. *et al.* A carnosine analog mitigates metabolic disorders of obesity
361 by reducing carbonyl stress. *J Clin Invest* **128**, 5280-5293, doi:10.1172/JCI94307
362 (2018).
363 8 Bhattacharya, A. *et al.* Denervation induces cytosolic phospholipase A2-mediated
364 fatty acid hydroperoxide generation by muscle mitochondria. *J Biol Chem* **284**, 46-
365 55, doi:10.1074/jbc.M806311200 (2009).
366 9 Pharaoh, G. *et al.* Targeting cPLA2 derived lipid hydroperoxides as a potential
367 intervention for sarcopenia. *Sci Rep* **10**, 13968, doi:10.1038/s41598-020-70792-7
368 (2020).
369 10 Kagan, V. E. *et al.* Oxidized arachidonic and adrenic PEs navigate cells to
370 ferroptosis. *Nat Chem Biol* **13**, 81-90, doi:10.1038/nchembio.2238 (2017).
371 11 Eshima, H. *et al.* Neutralizing mitochondrial ROS does not rescue muscle atrophy
372 induced by hindlimb unloading in female mice. *J Appl Physiol (1985)* **129**, 124-132,
373 doi:10.1152/japplphysiol.00456.2019 (2020).
374 12 Heden, T. D. *et al.* Mitochondrial PE potentiates respiratory enzymes to amplify
375 skeletal muscle aerobic capacity. *Sci Adv* **5**, eaax8352, doi:10.1126/sciadv.aax8352
376 (2019).
377 13 Yant, L. J. *et al.* The selenoprotein GPX4 is essential for mouse development and
378 protects from radiation and oxidative damage insults. *Free Radic Biol Med* **34**, 496-
379 502, doi:10.1016/s0891-5849(02)01360-6 (2003).
380 14 Katunga, L. A. *et al.* Obesity in a model of gpx4 haploinsufficiency uncovers a
381 causal role for lipid-derived aldehydes in human metabolic disease and
382 cardiomyopathy. *Mol Metab* **4**, 493-506, doi:10.1016/j.molmet.2015.04.001 (2015).
383 15 Yoo, S. E. *et al.* Gpx4 ablation in adult mice results in a lethal phenotype
384 accompanied by neuronal loss in brain. *Free Radic Biol Med* **52**, 1820-1827,
385 doi:10.1016/j.freeradbiomed.2012.02.043 (2012).
386 16 Imai, H. & Nakagawa, Y. Biological significance of phospholipid hydroperoxide
387 glutathione peroxidase (PHGPx, GPx4) in mammalian cells. *Free Radic Biol Med*
388 **34**, 145-169, doi:10.1016/s0891-5849(02)01197-8 (2003).
389 17 Lee, J. Y., Kim, W. K., Bae, K. H., Lee, S. C. & Lee, E. W. Lipid Metabolism and
390 Ferroptosis. *Biology (Basel)* **10**, doi:10.3390/biology10030184 (2021).
391 18 Ferrara, P. J. *et al.* Lysophospholipid acylation modulates plasma membrane lipid
392 organization and insulin sensitivity in skeletal muscle. *J Clin Invest* **131**,
393 doi:10.1172/JCI135963 (2021).
394 19 Ferrara, P. J. *et al.* Low lysophosphatidylcholine induces skeletal muscle myopathy
395 that is aggravated by high-fat diet feeding. *FASEB J* **35**, e21867,
396 doi:10.1096/fj.202101104R (2021).

397 20 Ran, Q. *et al.* Transgenic mice overexpressing glutathione peroxidase 4 are
398 protected against oxidative stress-induced apoptosis. *J Biol Chem* **279**, 55137-
399 55146, doi:10.1074/jbc.M410387200 (2004).
400 21 Dixon, S. J. *et al.* Ferroptosis: an iron-dependent form of nonapoptotic cell death.
401 *Cell* **149**, 1060-1072, doi:10.1016/j.cell.2012.03.042 (2012).
402 22 Codenotti, S. *et al.* Cell growth potential drives ferroptosis susceptibility in
403 rhabdomyosarcoma and myoblast cell lines. *J Cancer Res Clin Oncol* **144**, 1717-
404 1730, doi:10.1007/s00432-018-2699-0 (2018).
405 23 Cripps, M. J. *et al.* Carnosine scavenging of glucolipotoxic free radicals enhances
406 insulin secretion and glucose uptake. *Sci Rep* **7**, 13313, doi:10.1038/s41598-017-
407 13649-w (2017).
408 24 Everaert, I., De Naeyer, H., Taes, Y. & Derave, W. Gene expression of carnosine-
409 related enzymes and transporters in skeletal muscle. *Eur J Appl Physiol* **113**, 1169-
410 1179, doi:10.1007/s00421-012-2540-4 (2013).
411 25 Boldyrev, A. A., Aldini, G. & Derave, W. Physiology and pathophysiology of
412 carnosine. *Physiol Rev* **93**, 1803-1845, doi:10.1152/physrev.00039.2012 (2013).
413 26 Gao, H. *et al.* Ferroptosis is a lysosomal cell death process. *Biochem Biophys Res*
414 *Commun* **503**, 1550-1556, doi:10.1016/j.bbrc.2018.07.078 (2018).
415 27 Ichimura, Y. *et al.* A ubiquitin-like system mediates protein lipidation. *Nature* **408**,
416 488-492, doi:10.1038/35044114 (2000).
417 28 Chen, X., Yu, C., Kang, R., Kroemer, G. & Tang, D. Cellular degradation systems in
418 ferroptosis. *Cell Death Differ* **28**, 1135-1148, doi:10.1038/s41418-020-00728-1
419 (2021).
420 29 Gao, M. *et al.* Ferroptosis is an autophagic cell death process. *Cell Res* **26**, 1021-
421 1032, doi:10.1038/cr.2016.95 (2016).
422 30 Cai, J. *et al.* Autophagy Ablation in Adipocytes Induces Insulin Resistance and
423 Reveals Roles for Lipid Peroxide and Nrf2 Signaling in Adipose-Liver Crosstalk.
424 *Cell Rep* **25**, 1708-1717 e1705, doi:10.1016/j.celrep.2018.10.040 (2018).
425 31 McCarthy, J. J., Srikuea, R., Kirby, T. J., Peterson, C. A. & Esser, K. A. Inducible
426 Cre transgenic mouse strain for skeletal muscle-specific gene targeting. *Skelet*
427 *Muscle* **2**, 8, doi:10.1186/2044-5040-2-8 (2012).
428 32 Ferrara, P. J., Verkerke, A. R. P., Brault, J. J. & Funai, K. Hypothermia Decreases
429 O2 Cost for Ex Vivo Contraction in Mouse Skeletal Muscle. *Med Sci Sports Exerc*
430 **50**, 2015-2023, doi:10.1249/MSS.0000000000001673 (2018).
431 33 Verkerke, A. R. P. *et al.* Phospholipid methylation regulates muscle metabolic rate
432 through Ca(2+) transport efficiency. *Nat Metab* **1**, 876-885, doi:10.1038/s42255-
433 019-0111-2 (2019).
434 34 Johnson, J. M. *et al.* Alternative splicing of UCP1 by non-cell-autonomous action of
435 PEMT. *Mol Metab* **31**, 55-66, doi:10.1016/j.molmet.2019.10.007 (2020).

436

437

Acknowledgements

This research is supported by NIH DK107397, GM144613, AG063077, University of Utah Center on Aging (to K.F.), AG050781 (to M.J.D.), HL122863, AG057006 (E.J.A), AG064078 (to Q.R.), HL149870 (S.B.), HL139451 (to Z.S.M), DK130555 (to A.D.P.), AG073493 (to J.J.P.), American Heart Association 18PRE33960491 (to A.R.P.V.) and 19PRE34380991 (to J.M.J.), Larry H. & Gail Miller Family Foundation (to P.J.F.), and Uehara Memorial Foundation (to H.E.). We would like to thank Diana Lim from the University of Utah Molecular Medicine Program for assistance with figures.

Author contributions

H.E. and K.F. contributed to study concept design and wrote the manuscript. P.S. and J.L.S. contributed to study design and data analysis. M.J.P., J.A.M., and J.E.C. performed mass spectrometry analyses. M.J.D. and Z.S.M. performed human muscle biopsies. H.E., P.S., J.L.S., A.W.L., J.M.J., J.J.P., and A.S., performed mouse experiments. H.E. performed all biochemical assays, body composition measurements and analysis of muscle force production. A.R.P.V. and P.J.F. assisted in muscle functional measurements. P.J.F. assisted in cell culture experiments. E.J.A assisted in L-carnosine and N-acetylcarnosine experiments. S.B. and Q.R. designed and generated mouse models. All contributed to editing the manuscript.

Competing interests

No competing interests to disclose.

Materials & Correspondence

Correspondence and material requests should be addressed to K. Funai.

463 **Figure legends**

464 **Fig. 1 | LOOH increases with aging and disuse in skeletal muscle. a**,**b** GPx4 mRNA
465 levels in skeletal muscle biopsy samples from young and old humans (*n* = 9 for young, *n* =
466 18 for old) (**a**) or skeletal muscles from young and old mice (*n* = 8 for young, *n* = 7 for old)
467 (**b**). **c**,**d**, Oxidized phospholipid content in skeletal muscle from young and old mice (*n* = 8
468 per group). **e**,**f**, Soleus muscle mass (**e**), force-frequency curve (**f**) in soleus muscle following
469 1 and 7 days of HU from young WT C57BL/6J mice (*n* = 4 for sham, *n* = 6 for 1 day HU, *n* =
470 6 for 7 day HU). **g**, Immunoblotting of 4-HNE following 1 and 7 days of HU. **h**. A schematic
471 on how pathways that regulate LOOH may promote muscle atrophy. PUFA: phospholipids
472 containing polyunsaturated fatty acids. **i**,**j**, Representative images (**i**), and quantification (**j**) of
473 myotube diameter (*n* = 104 for scrambled: SC, *n* = 107 for GPx4 KD, *n* = 117 for Vehicle, *n*
474 = 120 for erastin, *n* = 104 for Vehicle, *n* = 110 for RSL3). Scale bar, 100 μm. Data are shown
475 as the mean ± s.e.m. Statistical analyses in **a**,**b**,**c**,**d** and **j** were performed with an unpaired
476 two-tailed t-test. Statistical analyses in **e** were performed with a one-way ANOVA with
477 Dunnett's multiple comparisons test. Statistical analyses in **f** were performed with a two-way
478 ANOVA and multiple comparisons were performed using Tukey's multiple comparisons tests.

479

480 **Fig. 2 | Elevated LOOH is sufficient to augment disuse-induced muscle atrophy in**
481 **young and old mice. a**, Soleus muscle mass from young or old WT or GPx4+/- mice with or
482 without HU (*n* = 8-11 per young group, *n* = 4-8 per old mice group). **b**, Force-frequency curve
483 from old WT or GPx4+/- mice (*n* = 4-7 per group). **c**, Immunoblotting of 4-HNE from old WT
484 or GPx4+/- mice. **d**, mRNA levels of GPx4 from young control or GPx4-MKO mice (*n* = 4 per
485 group). **e**,**f**, Soleus muscle mass (**e**) (*n* = 7-8 per group) or force-frequency curve (**f**) from
486 young control or GPx4-MKO mice (*n* = 4-7 per group). **g**, Immunoblotting of 4-HNE and GPx4
487 from young GPx4-MKO. **h**,**i**, Representative images of MHC immunofluorescence (**h**) and
488 muscle fiber CSA by fiber type (**i**) for soleus muscles in young control or GPx4-MKO mice
489 with HU (*n* = 4 per group). **j**, Immunoblotting of 4-HNE, GPx4 and Actin protein in C2C12
490 myotubes with or without GPx4 KD and/or LPCAT3 KD. **k**,**l**, Representative images (**k**), and
491 quantification of myotube diameter (**l**) from C2C12 myotubes with or without GPx4 KD and/or
492 without LPCAT3 KD (n = 104-114 per group). Scale bar, 100 μm. Data are shown as the
493 mean ± s.e.m. Statistical analyses in **d** were performed with an unpaired two-tailed t-test.
494 Statistical analyses in **l** were performed with a one-way ANOVA with Dunnett's multiple
495 comparisons test. Statistical analyses in **a**,**c**,**e**,**f**, and **i** were performed with a two-way
496 ANOVA and multiple comparisons were performed using Tukey's (**c**,**e**,**f**,**i**) or Sidak's (**a**)
497 multiple comparisons tests.

498

499 **Fig. 3 | Genetic and pharmacologic suppression of LOOH ameliorates muscle atrophy**
500 **and weakness in young and old mice. a**, Soleus muscle mass from young or old WT or
501 GPx4Tg mice with or without HU (*n* = 6-11 per young group, *n* = 7 per old group). **b**, Force-
502 frequency curve from old WT or GPx4Tg mice (*n* = 5-7 per group). **c**, Immunoblotting of
503 muscle 4-HNE from old WT or GPx4Tg mice. **d**,**e**, Representative images of MHC
504 immunofluorescence (**d**) and muscle fiber CSA by fiber type (**e**) for soleus muscles in old WT
505 or GPx4Tg mice with HU (*n* = 4-6 per group). **f**, Immunoblotting of 4-HNE, and actin in C2C12
506 myotubes with or without GPx4 KD and/or Ferrostatin-1. **g**,**h**, Representative images (**g**), and
507 quantification of myotube diameter (**h**) from C2C12 myotubes with GPx4 KD and/or
508 Ferrostatin-1 treatments (*n* = 102-110 per group). Scale bar, 100 μm. **i**, Schematic illustration
509 of the protocol for administration of N-acetylcarnosine in vivo. **j**, Immunoblotting of muscle 4-
510 HNE from N-acetylcarnosine treatment in old mice. **k**, Soleus muscle mass from young or
511 old mice with or without N-acetylcarnosine treatment (*n* = 6-8 per young group, *n* = 7 per old
512 group). **l**, Force-frequency curve from N-acetylcarnosine study in old mice (*n* = 4-5 per group).
513 **m**,**n**, Representative images of MHC immunofluorescence (**m**) and muscle fiber CSA by fiber
514 type (**n**) for soleus muscles (*n* = 3-4 per group) in old mice from the N-acetylcarnosine study.
515 Data are shown as the mean ± s.e.m. Statistical analyses in **h** was performed with a one-
516 way ANOVA with Dunnett's multiple comparisons test, and Statistical analyses in **a**,**b**,**e**,**k**,**l**,
517 and **n** were performed with a two-way ANOVA and were performed using Tukey's (**b**,**e**,**l**,**n**)
518 or Sidak's (**a**,**k**) multiple comparisons tests.

519

520 **Fig. 4 | Autophagy-lysosomal system amplifies LOOH to promote muscle atrophy. a**,**b**,
521 Representative images (**a**), and quantification of myotube diameter (**b**) from erastin-
522 stimulated C2C12 myotubes with proteasomal inhibitor MG132 or lysosomal inhibitor BaFA1.
523 (*n* = 21-120 per group). Scale bar, 100 μm. **c**, Autophagic flux analyses immunoblotting for
524 LC3-I, LC3-II, p62, and actin in SC or GPx4 KD C2C12 myotuebs with or without BafA1. **d**,**e**,
525 Representative images (**d**) and quantification of myotube diameter (**e**) from C2C12 myotubes
526 with or without GPx4 KD and/or ATG3 KD) (n = 104-121 per group). **f**, mRNA levels of ATG3
527 (*n* = 8-32 per group) from young control or ATG3-MKO mice. **g**, Soleus muscle mass from
528 control or ATG3-MKO mice (*n* = 10-12 per group). **h**, Force-frequency curve from young
529 control or ATG3-MKO mice (*n* = 9-12 per group). **i**,**j**, Representative images of MHC
530 immunofluorescence (**i**) and muscle fiber CSA by fiber type (**j**) of soleus muscles in young
531 control or ATG3-MKO mice with HU (*n* = 6 per group). **k**, Immunoblotting of 4-HNE, GPx4,
532 and actin in C2C12 myotubes with or without GPx4 KD and/or ATG3 KD. **l**, Confocal

533 immunofluorescence of LAMP2 (lysosome) and 4-HNE in erastin-stimulated C2C12
534 myotubes with or without BaFA1. **m**, Representative images of H_2O_2 or BCNU-stimulated
535 C2C12 myotubes with or without BaFA1. Scale bar, 100 μm. **n**, Immunoblotting of 4-HNE
536 and actin in H_2O_2-stimulated C2C12 myotubes with or without BafA1. **o**, A novel role of
537 lysosome in amplifying LOOH. Data are shown as the mean ± s.e.m. Statistical analyses in
538 **f** were performed with an unpaired two-tailed t-test. Statistical analyses in **b**,**e** was performed
539 with a one-way ANOVA with Dunnett's multiple comparisons test, and **g**,**h**, and **j** were
540 performed with a two-way ANOVA and multiple comparisons were performed using Tukey's
541 multiple comparisons tests.

542 **Extended Data Fig. 1** (Related to age or disuse experiments in Figure 1). (**a**) Immunoblotting
543 of 4-HNE and GPx4 in skeletal muscle from young and old C57BL6/J mice. (**b**,**c**)
544 Quantification of 4- HNE (**b**) and MDA levels (**c**) (*n* = 5 per group) in young and old C57BL6/J
545 mice. (**d-f**) body mass (**d**), body composition (**e**), food intake (**f**), following 1, and 7 days of
546 HU from young WT C57BL/6J mice (*n* = 4 for sham, *n* = 6 for 1day HU, *n* = 6 for 7day HU).
547 (**g**) Quantification of 4- HNE (*n* = 3 per group). (**h**) Rates of oxygen consumption measured
548 in isolated skeletal muscle mitochondria with Krebs cycle substrates (n = 4 for sham, n = 5
549 for 1 day HU, n = 5 for 7 day HU). ADP, adenosine diphosphate; FCCP, carbonyl cyanide-p-
550 trifluoromethoxyphenylhydrazone; Mal, malate; Pyr, pyruvate. (**i**) Rate of mitochondrial H_2O_2
551 production in response to succinate or Aurorafin/BCNU (n = 4 for sham, n = 5 for 1 day HU,
552 n = 5 for 7 day HU). BCNU, 1,3-bis[2-chloroethyl]-1-nitrosourea. (**j**) Percentage of electron
553 leak in muscle mitochondria (n = 4 for sham, n = 5 for 1 day HU, n = 5 for 7 day HU). Data
554 are shown as the mean ± s.e.m. Statistical analyses in **b** and **c** were performed with an
555 unpaired two-tailed t-test. Statistical analyses in **d**,**e**,**f**,**g**, and **j** were performed with an one-
556 way ANOVA and Dunnett's multiple comparisons tests. Statistical analyses in **h**, and **i** were
557 performed with a two-way ANOVA and Tukey's multiple comparison test.

558

559 **Extended Data Fig. 2** (Related to in vitro experiments in Figure 1). (**a**) GPx4 mRNA levels
560 in C2C12 myotubes with or without GPx4 knockdown (GPx4 KD) (n = 6 per group). (**b-d**)
561 Immunoblotting of 4-HNE, GPx4, and actin (**b**), quantification of 4-HNE (**c**) proteins and MDA
562 levels (**d**) (n = 3 per group). (**e**) mRNA levels for CHAC1 and PTGS2 (n = 6 per group). (**f**)
563 cell death levels in GPx4 KD myoblast or myotubes (n = 3 independent repeats). (**g-k**)
564 Quantification of 4-HNE (**g**), immunoblotting of 4-HNE (**h**) proteins, MDA levels (**i**), mRNA
565 levels for CHAC1 and PTGS2 (**j**), and cell death levels (**k**) in erastin-stimulated C2C12
566 myotubes (n = 3 independent repeats). (**l-o**) mRNA levels of GPx4 (**l**), immunoblotting of
567 GPx4 and actin (**m**), quantification of GPx4 (**n**), CHAC1 and PTGS2 (**o**) in RSL3-stimulated
568 C2C12 myotubes (n = 6 per group). Data are shown as the mean ± s.e.m. Statistical analyses
569 in **a**,**c**,**d**,**f**,**i**,**j**,**k**,**l**,**n** and **o** were performed with an unpaired two-tailed t-test. Statistical analyses
570 in **g** were performed with a one-way ANOVA and Dunnett's multiple comparisons tests.
571 Statistical analyses in **e** were performed with a two-way ANOVA and Tukey's multiple
572 comparison test.

573

574 **Extended Data Fig. 3** (Related to GPx4+/- mice in Figure 2). (**a**) Body mass from young and
575 old WT or GPx4+/- mice. (**b**,**c**) body composition from young (n = 9 for WT sham, n = 8 for

576 GPx4 +/- sham, n = 7 for WT HU, n = 6 for GPx4 +/- HU) (**b**) and old (n = 4 for WT sham, n
577 = 5 for GPx4 +/- sham, n = 8 for WT HU, n = 6 for GPx4 +/- HU) (**c**) WT or GPx4+/- mice. (**d**)
578 Food intake during hindlimb unloading (HU) in young (n = 7 for WT, n = 6 for GPx4 +/-) and
579 old (n = 8 for WT, n = 6 for GPx4 +/-) WT or GPx4+/- mice. (**e**) EDL muscle mass from young
580 (n = 9 for WT sham, n = 8 for GPx4 +/- sham, n = 7 for WT HU, n = 6 for GPx4 +/- HU) and
581 old (n = 9 for WT sham, n = 8 for GPx4 +/- sham, n = 7 for WT HU, n = 6 for GPx4 +/- HU)
582 WT or GPx4+/- mice. (**f**) Quantification of muscle 4-HNE from old mice (n = 3 per group). (**g**)
583 MDA levels from old mice (n = 3 per group). (**h**) Force-frequency curve from soleus muscle
584 from young WT or GPx4+/- mice (n = 5 for WT sham, n = 5 for GPx4 +/- sham, n = 7 for WT
585 HU, n = 5 for GPx4 +/- HU). (**i**,**j**) Force-frequency curve in EDL muscle from young (n = 5 for
586 WT sham, n = 5 for GPx4 +/- sham, n = 7 for WT HU, n = 5 for GPx4 +/- HU) (**i**) and old (n =
587 3 for WT sham, n = 4 for GPx4 +/- sham, n = 6 for WT HU, n = 6 for GPx4 +/- HU) (**j**) WT or
588 GPx4+/- mice. Data are shown as the mean ± s.e.m. Statistical analyses in **a-j** were
589 performed with a two-way ANOVA and using Tukey's multiple comparisons tests.

590

591 **Extended Data Fig. 4** (Related to GPx4-MKO mice in Figure 2). (**a**) Genotyping gel for
592 GPx4cKO+/+ mice crossed with HSA-MCM+/- mice to yield GPx4cKO+/+; HSA-MCM+/-
593 (GPx4-MKO) mice. Control littermates (GPx4cKO +/+; HSA-MCM -/-) were used for
594 experiments. Body mass (**b**), and body composition (**c**) (n = 7 for Ctrl sham, n = 4 for GPx4-
595 MKO sham, n = 7 for Ctrl HU, n = 8 for GPx4-MKO HU). (**d)** Food intake during HU (n = 7 for
596 Ctrl, n = 8 for GPx4-MKO). (**e**,**f**) EDL muscle mass (n = 6 for Ctrl sham, n = 4 for GPx4-MKO
597 sham, n = 7 for Ctrl HU, n = 8 for GPx4-MKO HU) (**e**) and force-frequency curve from young
598 mice (n = 6 for Ctrl sham, n = 4 for GPx4-MKO sham, n = 6 for Ctrl HU, n = 7 for GPx4-MKO
599 HU) (**f**). (**g**) Quantification of western blotting for 4-HNE from young mice (n = 3 per group).
600 (**h**) mRNA levels of CHAC1 and PTGS2 in skeletal muscles (n = 4 per group). (**i**,**j**) Mean
601 muscle fiber CSA (**i**) and fiber type composition (**j**) for soleus muscles following HU (*n* = 4
602 per group). Data are shown as the mean ± s.e.m. Statistical analyses in **d**, and **i**, were
603 performed with an unpaired two-tailed t-test. Statistical analyses in **b**,**c**,**e**,**f**,**g**,**h** and **j** were
604 performed with a two-way ANOVA and Tukey's multiple comparison test.

605

606 **Extended Data Fig. 5** (Related to LPCAT3 KD studies in Figure 2). (**a**) mRNA levels of
607 LPCAT3 in C2C12 myotubes with or without LPCAT3 KD (n = 3 per group). (**b**) mRNA levels
608 of GPx4 and LPCAT3 in C2C12 myotubes with double knockdown for GPx4 and LPCAT3 (n
609 = 3 per group). (**c**) Quantification of 4-HNE proteins in C2C12 myotubes with or without

610 LPCAT3 KD and/or GPx4 KD (n=3 per group). (**d**,**e**) immunoblotting (**d**) and quantification
611 (**e**) of 4-HNE from C2C12 myotubes with or without LPCAT 3 KD and/or erastin (n = 3 per
612 group). (**f**) mRNA levels of LPCAT3 from erastin-stimulated myotubes (n = 3 per group). (**g**,**h**)
613 Representative images of myotubes (**g**) and cell death levels (**h**) from C2C12 myotubes with
614 or without LPCAT3 KD and/or erastin (n = 3 independent repeats). Scale bar, 100 μm. Data
615 are shown as the mean ± s.e.m. Statistical analyses in **a**,**b**, and **f** were performed with an
616 unpaired two-tailed t-test. Statistical analyses in **c**,**e**, and **h** were performed with a two-way
617 ANOVA and Tukey's multiple comparison test.

618

619 **Extended Data Fig. 6** (Related to GPx4Tg mice in Figure 3). (**a**) Quantification of GPx4
620 proteins from WT or GPx4Tg with or without HU (n = 3 per group). (**b**) Body mass from young
621 (n = 9 for WT, n = 8 for GPx4Tg) and old (n = 7 for WT, n = 7 for GPx4Tg) mice. (**c**,**d**) body
622 composition from young mice (**c**) and old mice (**d**). (**e**) Food intake during HU from young
623 and old mice. (**f**,**g**) EDL muscle mass from young (n = 6 for WT sham, n = 8 for GPx4Tg
624 sham, n = 9 for WT HU, n = 8 for GPx4Tg HU)(**f**) and old (n = 7 per group) (**g**) mice. (**h**)
625 Force-frequency curve in soleus muscle from young mice (n = 5 for WT sham, n = 6 for
626 GPx4Tg sham, n = 9 for WT HU, n = 8 for GPx4Tg HU). (**i**,**j**) Force-frequency curve in EDL
627 muscle from young mice (n = 5 for WT sham, n = 7 for GPx4Tg sham, n = 9 for WT HU, n =
628 8 for GPx4Tg HU) (**i**) and old (n = 5 for WT sham, n = 5 for GPx4Tg sham, n = 5 for WT HU,
629 n = 6 for GPx4Tg HU) (**j**) mice. (**k**) Quantification of muscle 4-HNE proteins from old mice (n
630 = 3 per group). (**l**,**m**) Mean muscle fiber CSA (**l**) and fiber type composition (**m**) for soleus
631 muscles from old mice following HU (*n* = 6 for WT, n = 4 for GPx4Tg). Data are shown as
632 the mean ± s.e.m. Statistical analyses in **l** were performed with an unpaired two-tailed t-test.
633 Statistical analyses in **a**-**m** were performed with a two-way ANOVA and Tukey's multiple
634 comparison test.

635

636 **Extended Data Fig. 7** (A pilot L-carnosine study leading to N-acetylcarnosine study in Figure
637 3). (**a**-**c**) Quantification of 4-HNE proteins (n = 2 per group) (**a**), cell death level (n = 3
638 independent repeats) (**b**), and mRNA levels of CHAC1 and PTGS2 with or without GPx4 KD
639 and/or Ferrostatin-1 (n = 6 for SC, n = 5 for GPx4 KD) (**c**) in C2C12 myotubes. (**d**-**f**)
640 Immunoblotting (**d**) and quantification (**e**) of 4-HNE, and actin (n = 3 per group) and cell death
641 level (n = 3 independent repeats) (**f**) with or without erastin and/or L-carnosine in C2C12
642 myotubes. (**g**-**i**) Immunoblotting (**g**) and quantification (**h**) of 4-HNE, and actin (n = 3 per
643 group), and (**i**) cell death level (n = 3 independent repeats) in C2C12 myotubes with or without
644 erastin and/or L-carnosine. (**j**-**p**) Administration of L-carnosine in young (4-month-old)

645 C57BL/6J mice with or without HU. Body mass (**j**), body composition (n = 6 for Vehicle sham,
646 n = 7 for L-carnosine sham, n = 12 for vehicle HU, n = 13 for L-carnosine HU) (**k**), food intake
647 (**l**), water intake (n = 6 for Vehicle sham, n = 6 for L-carnosine sham, n = 6 for vehicle HU, n
648 = 7 for L-carnosine HU) (**m**), immunoblotting (**n**) and quantification (**o**) of 4-HNE (n = 3 per
649 group), and soleus muscle mass (n = 6 for Vehicle sham, n = 7 for L-carnosine sham, n = 12
650 for vehicle HU, n = 13 for L-carnosine HU) (**p**). Data are shown as the mean ± s.e.m.
651 Statistical analyses in **e**, and **f** were performed with a one-way ANOVA and Tukey's multiple
652 comparison test. Statistical analyses in **a**,**b**,**c**,**h**,**i**,**j**,**k**,**l**,**m**,**o** and **p** were performed with a two-
653 way ANOVA and Tukey's multiple comparison test.

654

655 **Extended Data Fig. 8** (Related to N-acetylcarnosinestudies in Figure 3). (**a**-**c**)
656 Immunoblotting (**a**) and quantification (**b**) for 4-HNE, GPx4 and actin (n = 3 per group) and
657 cell death level (n = 3 independent repeats) (**c**) from C2C12 myotubes with or without GPx4
658 KD and/or N-acetylcarnosine. (**d**-**f**) Immunoblotting (**d**) and quantification (**e**) of 4-HNE and
659 actin (n = 3 per group) and cell death level (n = 3 independent repeats) (**f**) in C2C12 myotubes
660 with or without erastin and/or N-acetylcarnosine. (**g**-**s**) Administration of N-acetylcarnosine
661 from young (4-month-old) and old (20-month-old) C57BL/6J mice. Body mass (**g**), body
662 composition from young mice (**h**) and old mice (**i**). Food intake (**j**), water intake (**k**),
663 immunoblotting (**l**) and quantification (**m**) of 4-HNE (n = 3 per group). (**n**) EDL muscle mass
664 from young mice and old mice. (**o**) Force-frequency curve in soleus muscle from young mice
665 (n = 5 for vehicle sham, n = 6 for N-acetylcarnosine sham, n = 5 for vehicle HU, n = 5 for N-
666 acetylcarnosine HU). (**p**,**q**) Force-frequency curve in EDL muscle from young mice (n = 7 for
667 vehicle sham, n = 7 for N-acetylcarnosine sham, n = 6 for vehicle HU, n = 7 for N-
668 acetylcarnosine HU) (**p**) and old mice (n = 6 for vehicle sham, n = 7 for N-acetylcarnosine
669 sham, n = 6 for vehicle HU, n = 6 for N-acetylcarnosine HU) (**q**). (**r**,**s**) Average of muscle fiber
670 CSA (**r**) and fiber type composition (**s**) for soleus muscles from old mice following HU (*n* = 3
671 for vehicle, n = 4 for N-acetylcarnosine). Data are shown as the mean ± s.e.m. Statistical
672 analyses in **r** were performed with an unpaired two-tailed t-test. Statistical analyses in **e**, and
673 **f** were performed with a one-way ANOVA and Tukey's multiple comparison test. Statistical
674 analyses in **b**,**c**,**g**,**h**,**i**,**j**,**k**,**m**,**n**,**o**,**p**,**q**, and **s** were performed with a two-way ANOVA and
675 Tukey's multiple comparison test.

676

677 **Extended Data Fig. 9** (Related to in vitro experiments in Figure 4). (**a**) Cell death levels in
678 erastin-stimulated myotubes with MG132 or BaFA1 (n = 3 independent repeats). (**b**,**c**)
679 Representative images (**b**) and cell death level (**c**) in RSL3-stimulated myotubes with BaFA1

680 (n = 3 independent repeats). Immunoblotting (**d**) and quantification (**e**) of LC3-I, LC3-II, p62
681 (all static measurements without BafA1), and actin protein from C2C12 myotubes with or
682 without GPX4 KD (n = 4 per group). (**f**-**h**) quantification of western blotting for LC3-I (**f**), LC3-
683 II (**g**), and p62 (**h**) protein from GPx4 KD myotubes with or without BaFA1 (n = 3 per group).
684 (**i**) mRNA levels of ATG3 in C2C12 myotubes with or without (n = 3 per group). (**j**) mRNA
685 levels of GPx4 and ATG3 from C2C12 myotubes with double knockdown for ATG3 and GPx4
686 (n = 3 per group). (**k**,**l**) Immunoblotting (**k**) and quantification (**l**) of LC3, p62, and GPx4 protein
687 from C2C12 myotubes with or without ATG3 KD (n = 3 per group). Data are shown as the
688 mean ± s.e.m. Statistical analyses in **c**,**i** and **l** were performed with an unpaired two-tailed t-
689 test. Statistical analyses in **a** were performed with a one-way ANOVA and Tukey's multiple
690 comparison test. Statistical analyses in **e**,**f**,**g**,**h**,**i**, and **j** were performed with a two-way
691 ANOVA and Tukey's multiple comparison test.

692

693 **Extended Data Fig. 10** (Related to in vivo and in vitro experiments in Figure 4). (**a**)
694 Genotyping of ATG3cKO+/+ mice crossed with HSA-MCM+/- mice to yield ATG3cKO+/+;
695 HSA-MCM+/- (ATG3-MKO) mice. Control littermates (ATG3cKO +/+; HSA-MCM -/-) were
696 used for experiments. (**b**) Immunoblotting of p62, LC3, and GAPDH proteins from skeletal
697 muscles from control and ATG3-MKO mice. (**c**) Quantification of LC3-II/I ratio in muscles
698 from control and ATG3-MKO mice (n = 8 per group). (**d**) Body weight, (**e**) lean mass, and (**f**)
699 fat mass from control and ATG3-MKO mice (control sham n = 9, ATG3-MKO sham n = 10,
700 control HU n = 10, ATG3-MKO HU n = 10). (**g**) EDL muscle mass (control sham n = 10,
701 ATG3-MKO sham n = 12, control HU n = 10, ATG3-MKO HU n = 10). (**h**) Force frequency
702 curve for EDL muscle (control sham n = 9, ATG3-MKO sham n = 8, control HU n = 10, ATG3-
703 MKO HU n = 9). (**i**) Fiber type composition for SOL muscle (control HU n = 6, ATG3MKO HU
704 n = 6). (**j**) quantification of 4-HNE protein from C2C12 myotubes with or without GPx4 KD
705 and/or ATG3 KD (n = 3 per group). (**k**,**l**) Immunoblotting (**k**) and quantification (**l**) of 4-HNE
706 protein from C2C12 myotubes with or without erastin and/or ATG3 KD (n = 3 per group).
707 (**m**,**n**) Immunoblotting (**m**) and quantification (**n**) of 4-HNE protein from C2C12 myotubes with
708 or without erastin and/or BaFA1 (n = 3 per group). (**o**,**p**) Immunoblotting (**o**) and quantification
709 (**p**) of 4-HNE protein from C2C12 myotubes with or without RSL3 and/or BaFA1 (n = 3 per
710 group). (**q**) Confocal fluorescence microscope images of erastin-stimulated myotubes with or
711 without BaFA1. Boxed regions are shown enlarged at far right. 4-HNE protein from H_2O_2-
712 stimulated (**r**), or BCNU-stimulated (**s**,**t**) C2C12 myotubes with or without BafA1. Data are
713 shown as the mean ± s.e.m. Statistical analyses in **c**,**d**,**e**,**f**,**g**,**h**,**i**,**j**,**l**,**n**,**p**,**r** and **t** were performed
714 with a two-way ANOVA and Tukey's multiple comparison test.

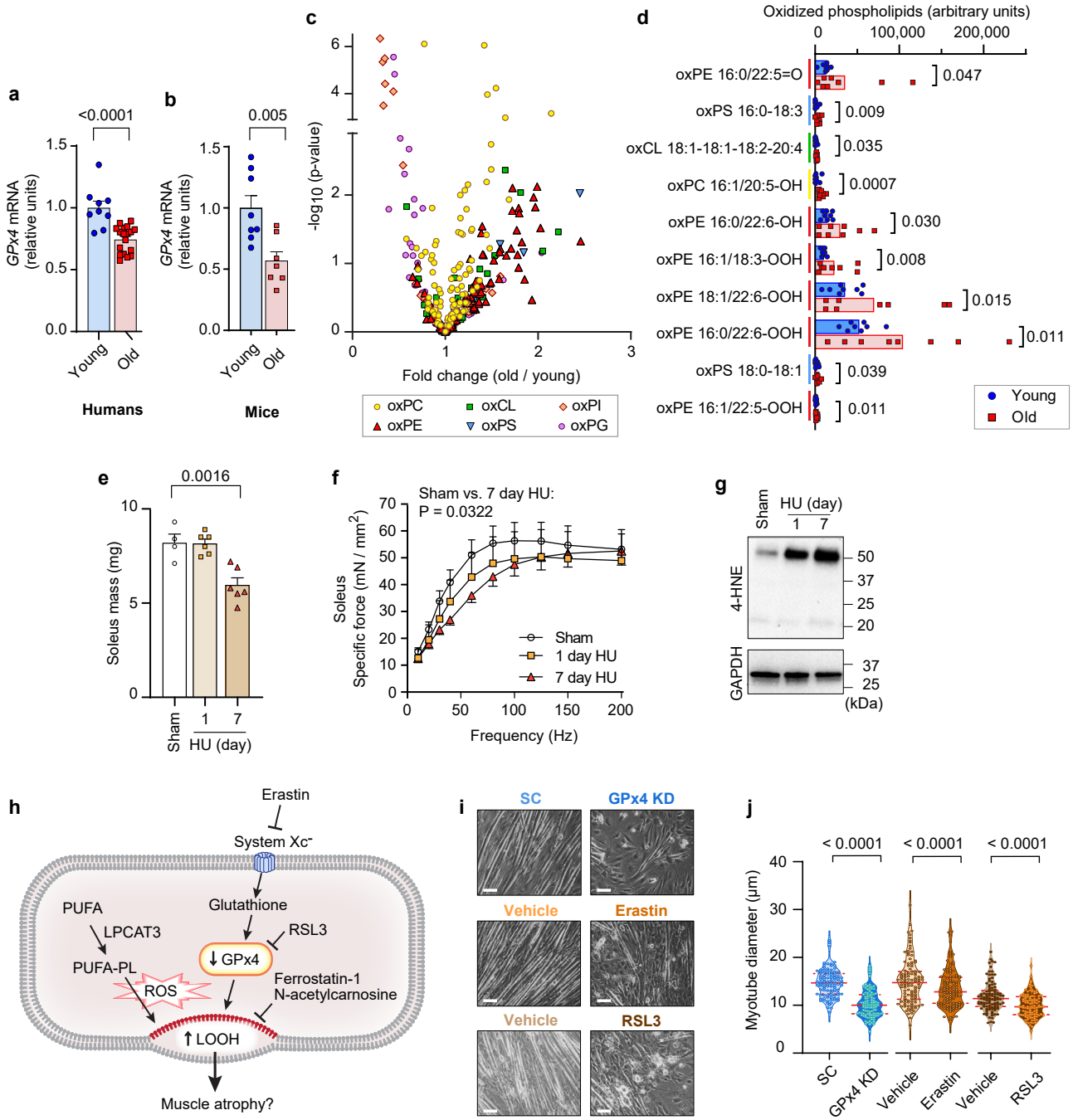
a
<0.0001
GPx4 mRNA (relative units)
Young
Old
Humans
b
0.005
Mice
c
-log10 (p-value)
Fold change (old / young)
oxPC
oxCL
oxPI
oxPE
oxPS
oxPG
d
Oxidized phospholipids (arbitrary units)
oxPE 16:0/22:5=O
oxPS 16:0-18:3
oxCL 18:1-18:1-18:2-20:4
oxPC 16:1/20:5-OH
oxPE 16:0/22:6-OH
oxPE 16:1/18:3-OOH
oxPE 18:1/22:6-OOH
oxPE 16:0/22:6-OOH
oxPS 18:0-18:1
oxPE 16:1/22:5-OOH
Young
Old
e
0.0016
Soleus mass (mg)
Sham
HU (day)
f
Sham vs. 7 day HU:
P = 0.0322
Soleus Specific force (mN / mm2)
Frequency (Hz)
Sham
1 day HU
7 day HU
g
Sham
HU (day)
4-HNE
GAPDH
(kDa)
h
Erastin
System Xc-
PUFA
LPCAT3
PUFA-PL
Glutathione
RSL3
GPx4
ROS
Ferrostatin-1
N-acetylcarnosine
LOOH
Muscle atrophy?
i
SC
GPx4 KD
Vehicle
Erastin
Vehicle
RSL3
j
< 0.0001
< 0.0001
< 0.0001
Myotube diameter (μm)
SC
GPx4 KD
Vehicle
Erastin
Vehicle
RSL3

Figure 1

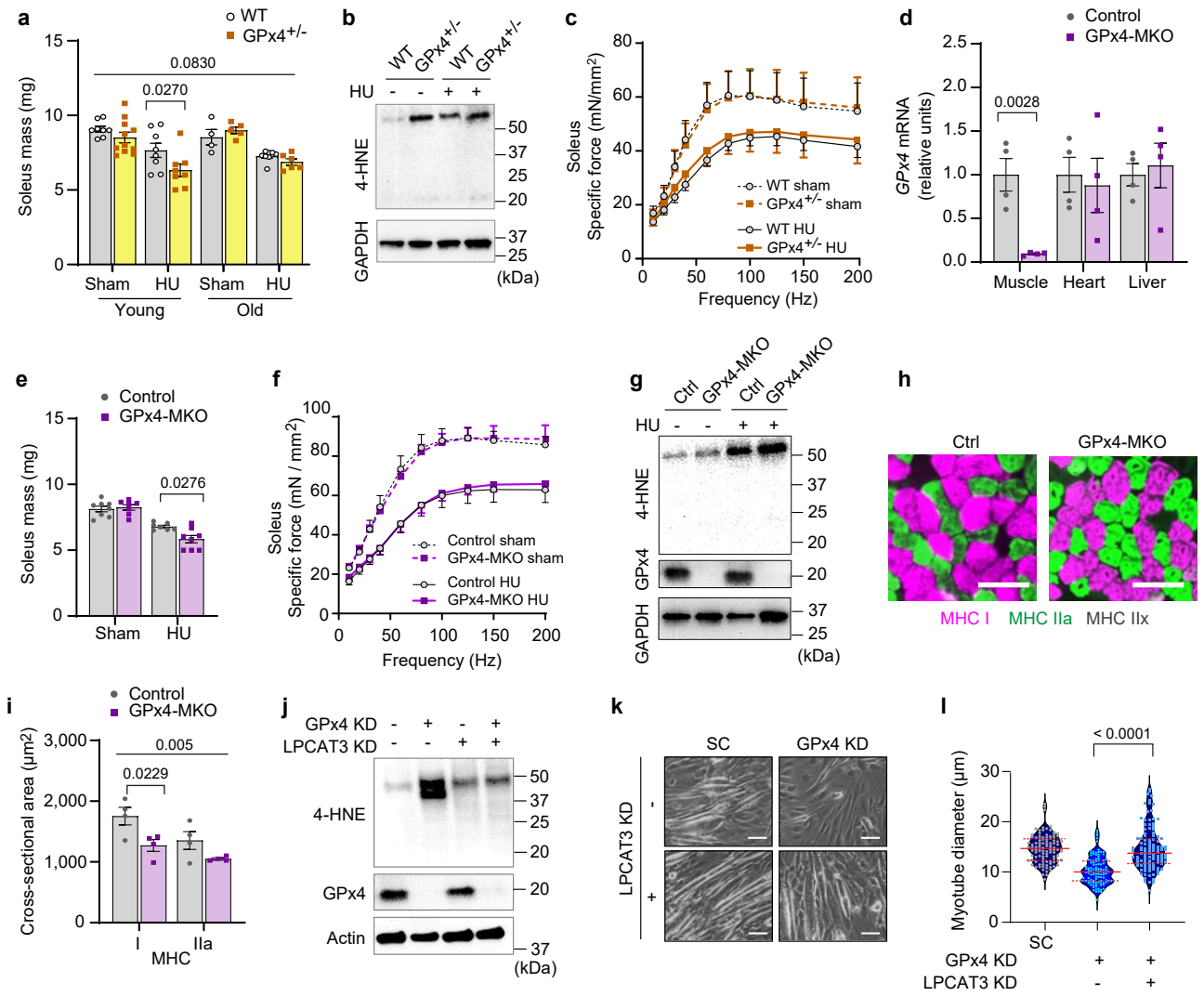
a
WT
GPx4+/-
Soleus mass (mg)
0.0830
0.0270
Sham
HU
Sham
HU
Young
Old
b
WT
GPx4+/-
WT
GPx4+/-
HU
4-HNE
GAPDH
(kDa)
c
Soleus
Specific force (mN/mm2)
WT sham
GPx4+/- sham
WT HU
GPx4+/- HU
Frequency (Hz)
d
Control
GPx4-MKO
GPx4 mRNA
(relative units)
0.0028
Muscle
Heart
Liver
e
Control
GPx4-MKO
Soleus mass (mg)
0.0276
Sham
HU
f
Soleus
Specific force (mN / mm2)
Control sham
GPx4-MKO sham
Control HU
GPx4-MKO HU
Frequency (Hz)
g
Ctrl
GPx4-MKO
Ctrl
GPx4-MKO
HU
4-HNE
GPx4
GAPDH
(kDa)
h
Ctrl
GPx4-MKO
MHC I
MHC IIa
MHC IIx
i
Control
GPx4-MKO
Cross-sectional area (μm2)
0.005
0.0229
I
IIa
MHC
j
GPx4 KD
LPCAT3 KD
4-HNE
GPx4
Actin
(kDa)
k
SC
GPx4 KD
LPCAT3 KD
l
< 0.0001
Myotube diameter (μm)
SC
GPx4 KD
LPCAT3 KD

Figure 2

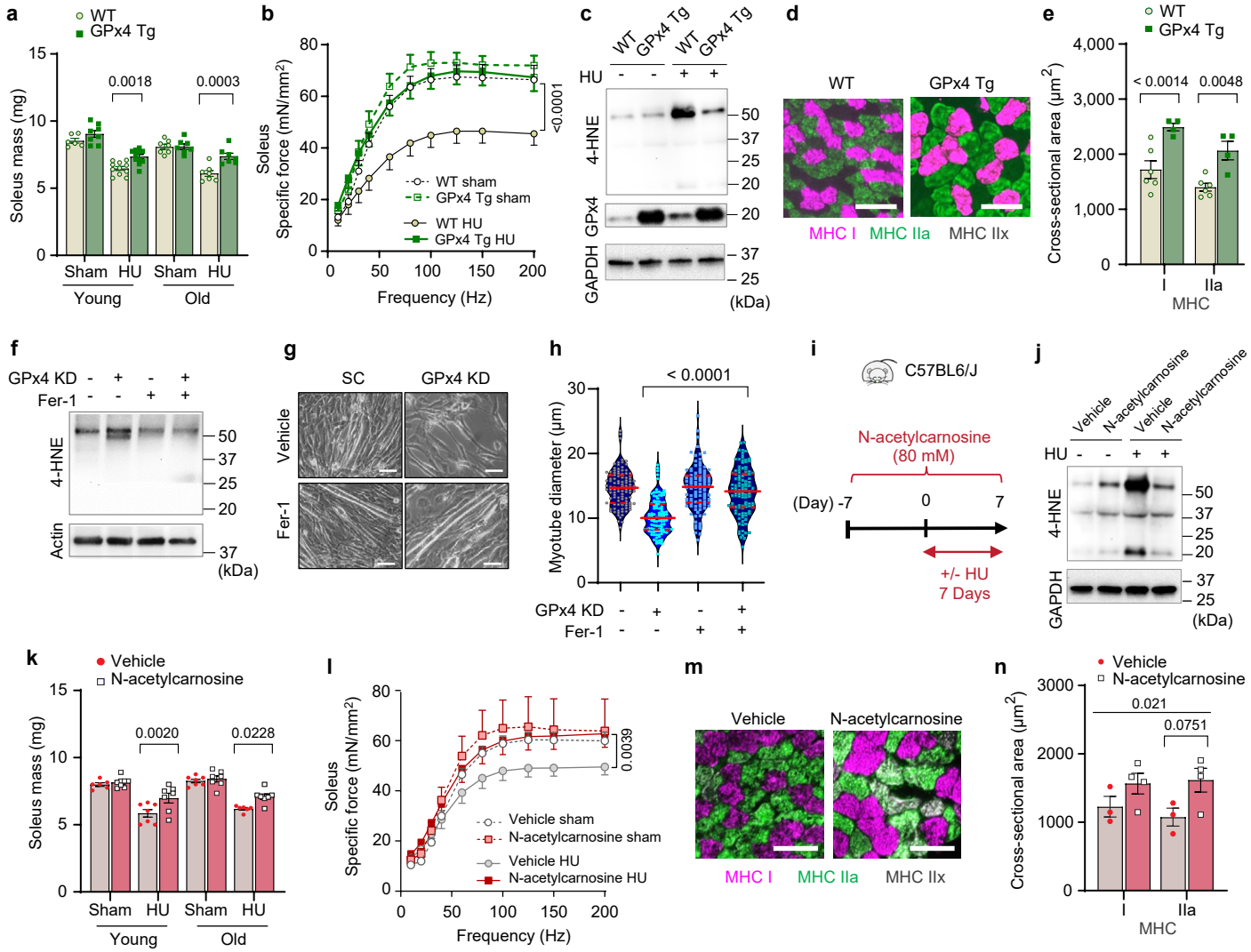
a
WT
GPx4 Tg
Soleus mass (mg)
0.0018
0.0003
Sham HU Sham HU
Young Old
b
Soleus Specific force (mN/mm²)
<0.0001
WT sham
GPx4 Tg sham
WT HU
GPx4 Tg HU
Frequency (Hz)
c
WT GPx4 Tg WT GPx4 Tg
HU
4-HNE
GPx4
GAPDH
(kDa)
d
WT
GPx4 Tg
MHC I MHC IIa MHC IIx
e
WT
GPx4 Tg
Cross-sectional area (μm²)
< 0.0014
0.0048
I IIa
MHC
f
GPx4 KD
Fer-1
4-HNE
Actin
(kDa)
g
SC
GPx4 KD
Vehicle
Fer-1
h
Myotube diameter (μm)
< 0.0001
GPx4 KD
Fer-1
i
C57BL6/J
N-acetylcarnosine (80 mM)
(Day) -7 0 7
+/- HU 7 Days
j
Vehicle N-acetylcarnosine Vehicle N-acetylcarnosine
HU
4-HNE
GAPDH
(kDa)
k
Vehicle
N-acetylcarnosine
Soleus mass (mg)
0.0020
0.0228
Sham HU Sham HU
Young Old
l
Soleus Specific force (mN/mm²)
0.0039
Vehicle sham
N-acetylcarnosine sham
Vehicle HU
N-acetylcarnosine HU
Frequency (Hz)
m
Vehicle
N-acetylcarnosine
MHC I MHC IIa MHC IIx
n
Vehicle
N-acetylcarnosine
Cross-sectional area (μm²)
0.021
0.0751
I IIa
MHC

Figure 3

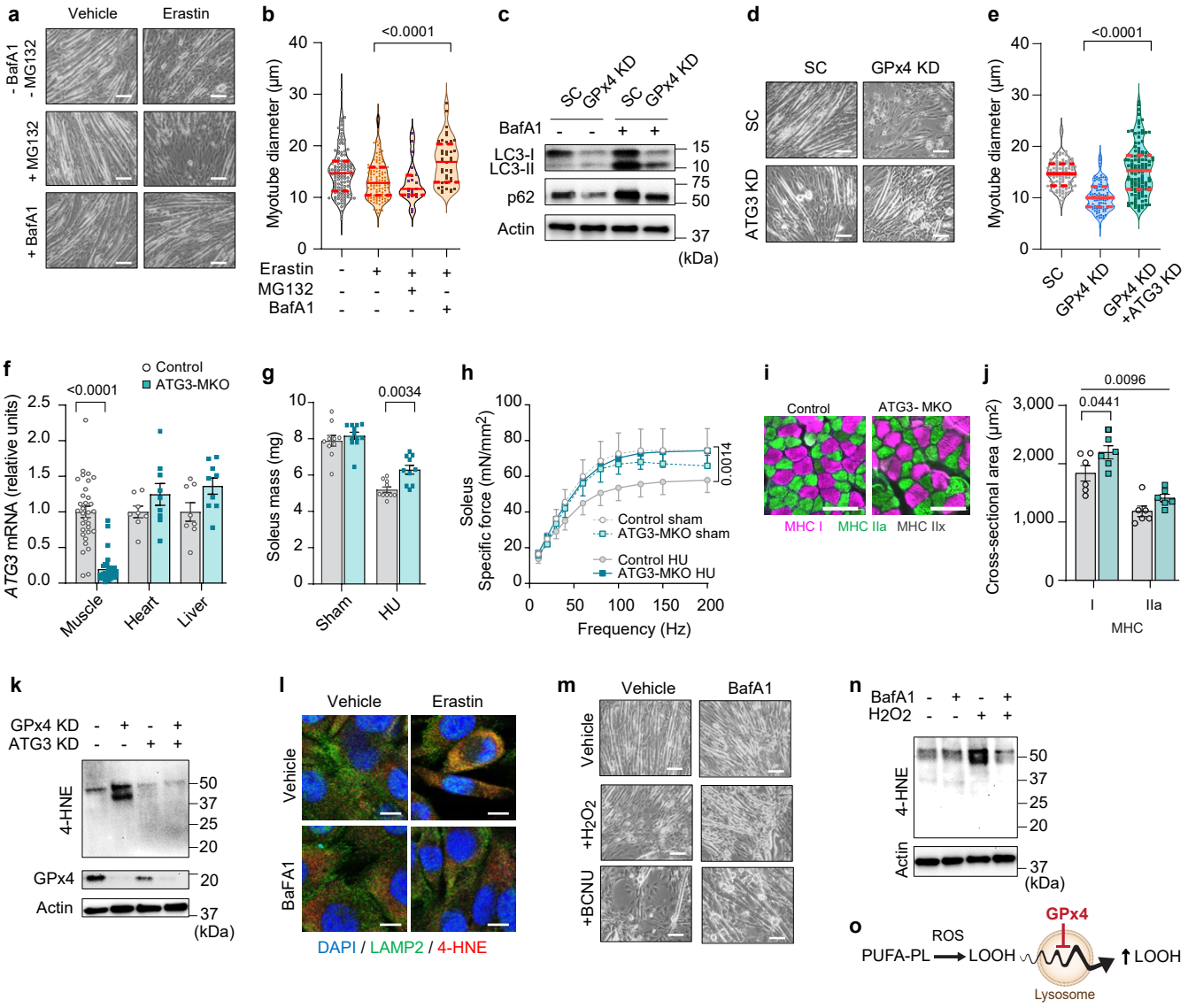
a
Vehicle
Erastin
- BafA1 - MG132
+ MG132
+ BafA1
b
<0.0001
Myotube diameter (μm)
Erastin
MG132
BafA1
c
SC
GPx4 KD
BafA1
LC3-I
LC3-II
p62
Actin
(kDa)
d
SC
GPx4 KD
ATG3 KD
e
<0.0001
Myotube diameter (μm)
SC
GPx4 KD
GPx4 KD +ATG3 KD
f
Control
ATG3-MKO
<0.0001
ATG3 mRNA (relative units)
Muscle
Heart
Liver
g
0.0034
Soleus mass (mg)
Sham
HU
h
Soleus Specific force (mN/mm2)
0.0014
Control sham
ATG3-MKO sham
Control HU
ATG3-MKO HU
Frequency (Hz)
i
Control
ATG3- MKO
MHC I
MHC IIa
MHC IIx
j
0.0096
0.0441
Cross-sectional area (μm2)
I
IIa
MHC
k
GPx4 KD
ATG3 KD
4-HNE
GPx4
Actin
(kDa)
l
Vehicle
Erastin
BaFA1
DAPI / LAMP2 / 4-HNE
m
Vehicle
BafA1
+H2O2
+BCNU
n
BafA1
H2O2
4-HNE
Actin
(kDa)
o
GPx4
ROS
PUFA-PL
LOOH
LOOH
Lysosome

Figure 4

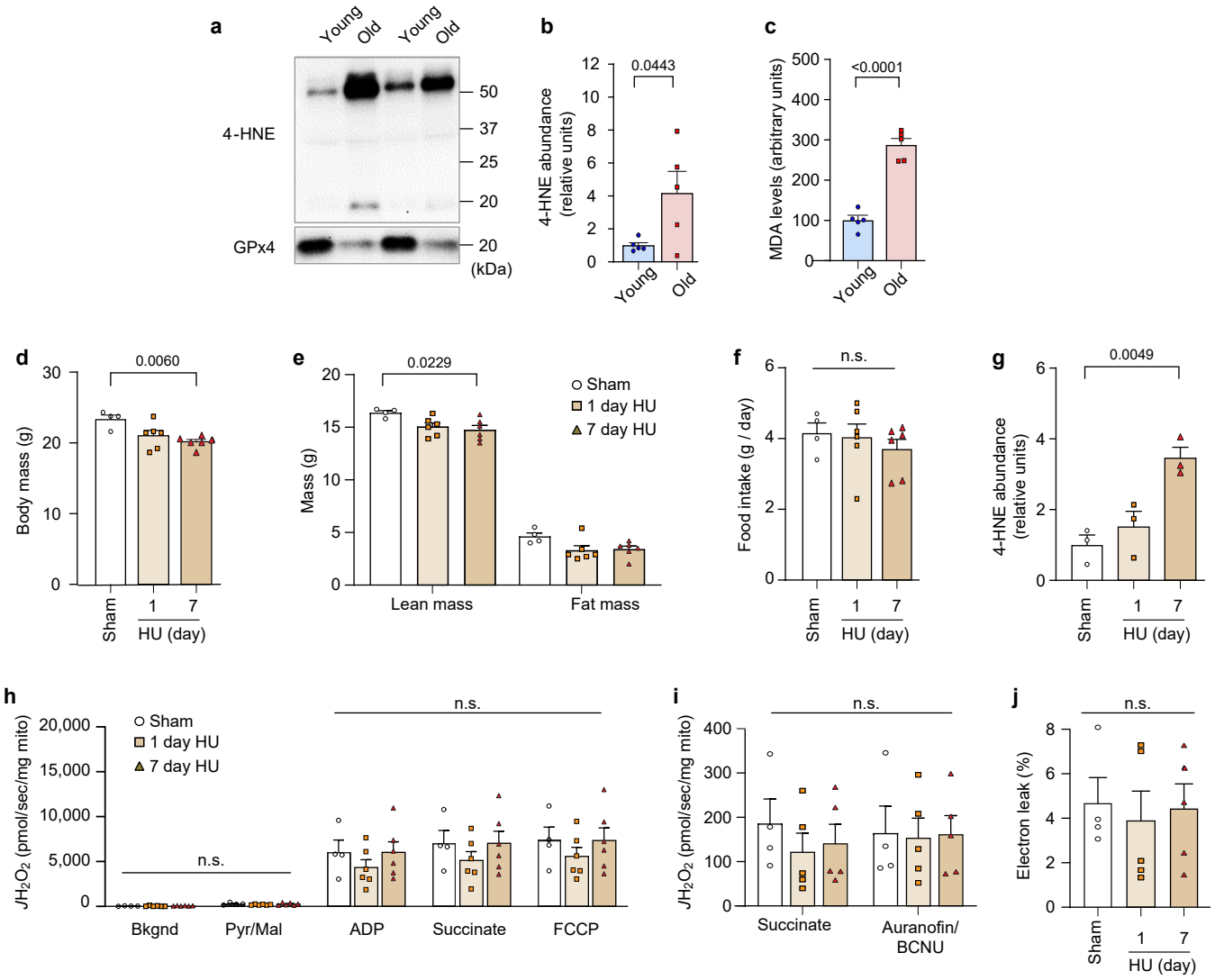
a
Young
Old
Young
Old
4-HNE
GPx4
50
37
25
20
20
(kDa)
b
0.0443
4-HNE abundance (relative units)
Young
Old
c
<0.0001
MDA levels (arbitrary units)
Young
Old
d
0.0060
Body mass (g)
Sham
1
7
HU (day)
e
0.0229
Mass (g)
Sham
1 day HU
7 day HU
Lean mass
Fat mass
f
n.s.
Food intake (g / day)
Sham
1
7
HU (day)
g
0.0049
4-HNE abundance (relative units)
Sham
1
7
HU (day)
h
Sham
1 day HU
7 day HU
n.s.
n.s.
JH2O2 (pmol/sec/mg mito)
Bkgnd
Pyr/Mal
ADP
Succinate
FCCP
i
n.s.
JH2O2 (pmol/sec/mg mito)
Succinate
Auranofin/ BCNU
j
n.s.
Electron leak (%)
Sham
1
7
HU (day)

ED 01

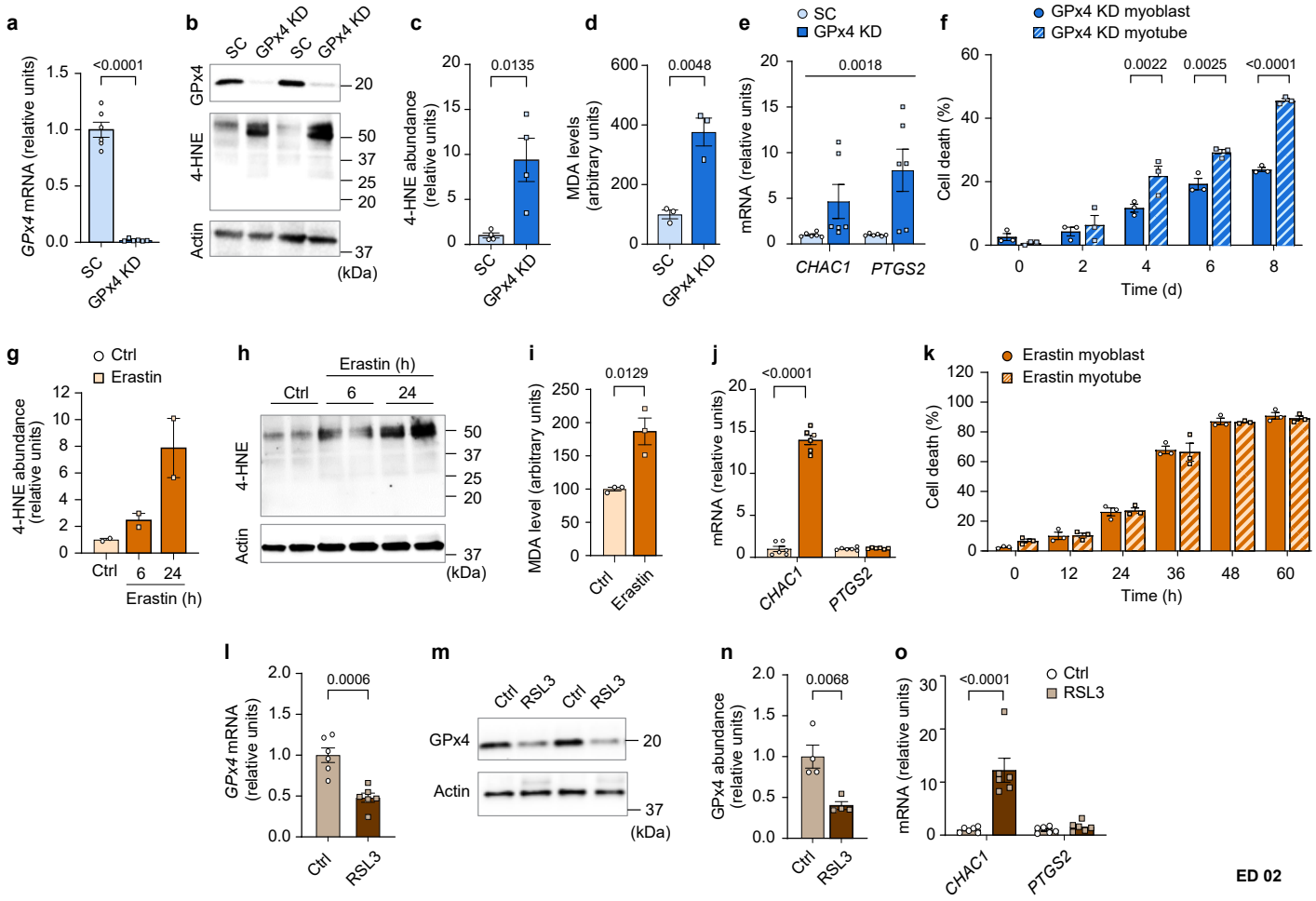
a
GPx4 mRNA (relative units)
<0.0001
SC
GPx4 KD
b
SC
GPx4 KD
SC
GPx4 KD
GPx4
4-HNE
Actin
20
50
37
25
20
37
(kDa)
c
4-HNE abundance (relative units)
0.0135
SC
GPx4 KD
d
MDA levels (arbitrary units)
0.0048
SC
GPx4 KD
e
SC
GPx4 KD
mRNA (relative units)
0.0018
CHAC1
PTGS2
f
GPx4 KD myoblast
GPx4 KD myotube
Cell death (%)
0.0022
0.0025
<0.0001
Time (d)
g
Ctrl
Erastin
4-HNE abundance (relative units)
Ctrl
6
24
Erastin (h)
h
Erastin (h)
Ctrl
6
24
4-HNE
Actin
50
37
25
20
37
(kDa)
i
MDA level (arbitrary units)
0.0129
Ctrl
Erastin
j
mRNA (relative units)
<0.0001
CHAC1
PTGS2
k
Erastin myoblast
Erastin myotube
Cell death (%)
Time (h)
l
GPx4 mRNA (relative units)
0.0006
Ctrl
RSL3
m
Ctrl
RSL3
Ctrl
RSL3
GPx4
Actin
20
37
(kDa)
n
GPx4 abundance (relative units)
0.0068
Ctrl
RSL3
o
mRNA (relative units)
<0.0001
Ctrl
RSL3
CHAC1
PTGS2
ED 02

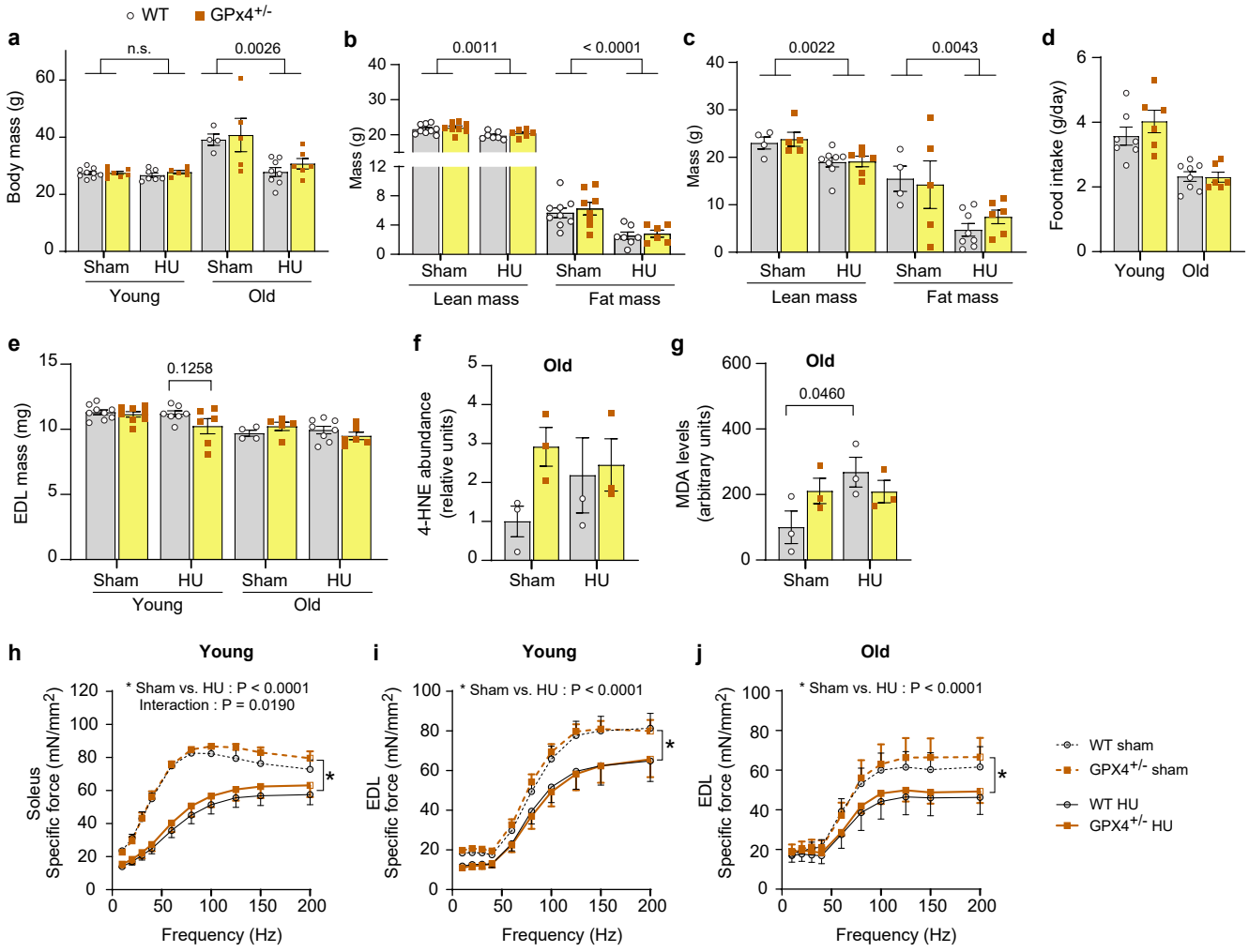
WT
GPx4+/-
a
n.s.
0.0026
Body mass (g)
Sham
HU
Young
Old
b
0.0011
< 0.0001
Mass (g)
Lean mass
Fat mass
c
0.0022
0.0043
d
Food intake (g/day)
e
0.1258
EDL mass (mg)
f
Old
4-HNE abundance (relative units)
g
0.0460
MDA levels (arbitrary units)
h
Young
* Sham vs. HU : P < 0.0001
Interaction : P = 0.0190
Soleus Specific force (mN/mm2)
Frequency (Hz)
i
* Sham vs. HU : P < 0.0001
EDL Specific force (mN/mm2)
j
WT sham
GPX4+/- sham
WT HU
GPX4+/- HU

ED 03

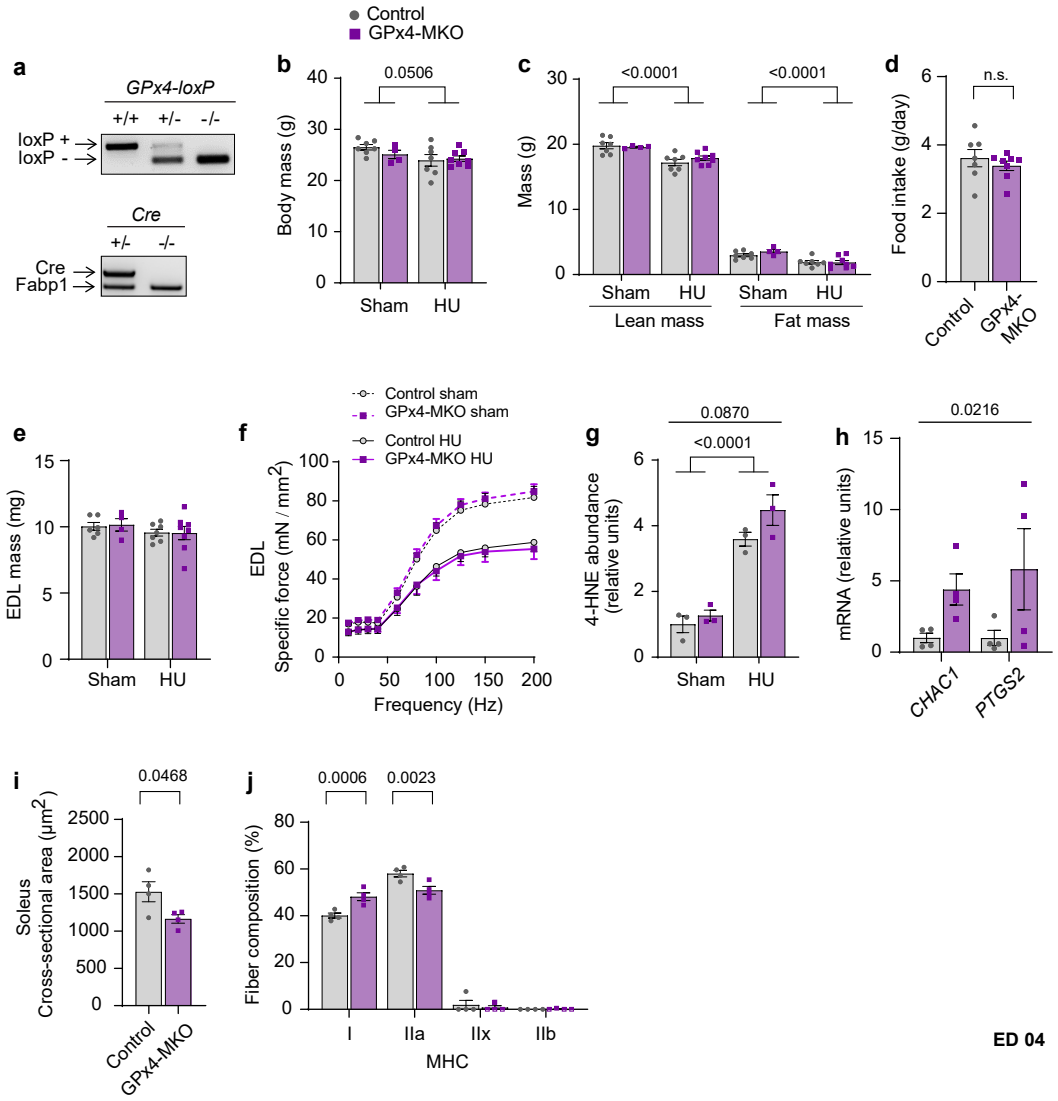
Control
GPx4-MKO
a
GPx4-loxP
+/+ +/- -/-
loxP +
loxP -
Cre
+/- -/-
Cre
Fabp1
b
0.0506
Body mass (g)
Sham HU
c
<0.0001
<0.0001
Mass (g)
Sham HU Sham HU
Lean mass Fat mass
d
n.s.
Food intake (g/day)
Control GPx4-MKO
e
EDL mass (mg)
Sham HU
f
Control sham
GPx4-MKO sham
Control HU
GPx4-MKO HU
EDL Specific force (mN / mm2)
Frequency (Hz)
g
0.0870
<0.0001
4-HNE abundance (relative units)
Sham HU
h
0.0216
mRNA (relative units)
CHAC1 PTGS2
i
0.0468
Soleus Cross-sectional area (μm2)
Control GPx4-MKO
j
0.0006 0.0023
Fiber composition (%)
I IIa IIx IIb
MHC
ED 04

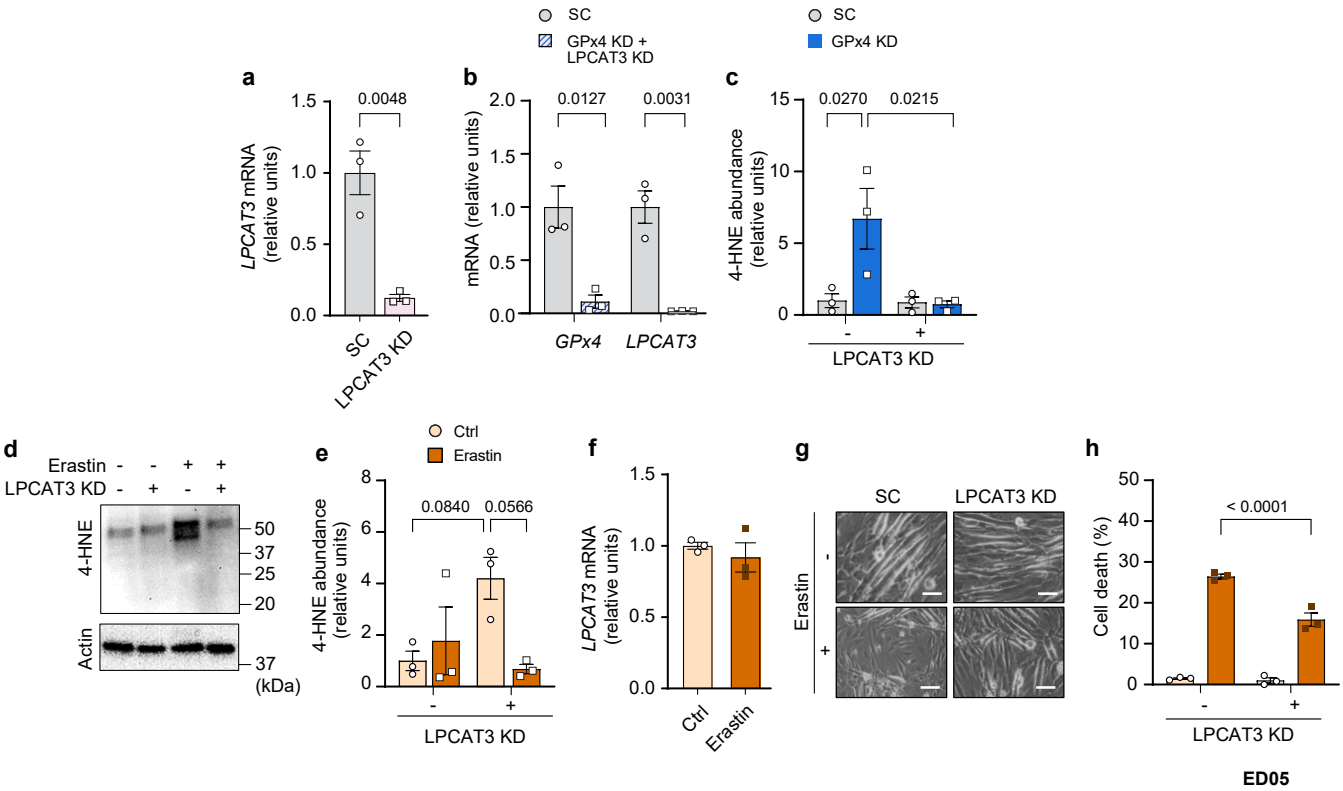
a
b
c
SC
GPx4 KD + LPCAT3 KD
GPx4 KD
LPCAT3 mRNA (relative units)
0.0048
SC
LPCAT3 KD
mRNA (relative units)
0.0127
0.0031
GPx4
LPCAT3
4-HNE abundance (relative units)
0.0270
0.0215
LPCAT3 KD
d
Erastin
LPCAT3 KD
4-HNE
Actin
(kDa)
e
Ctrl
Erastin
4-HNE abundance (relative units)
0.0840
0.0566
LPCAT3 KD
f
LPCAT3 mRNA (relative units)
Ctrl
Erastin
g
SC
LPCAT3 KD
Erastin
h
Cell death (%)
< 0.0001
LPCAT3 KD
ED05

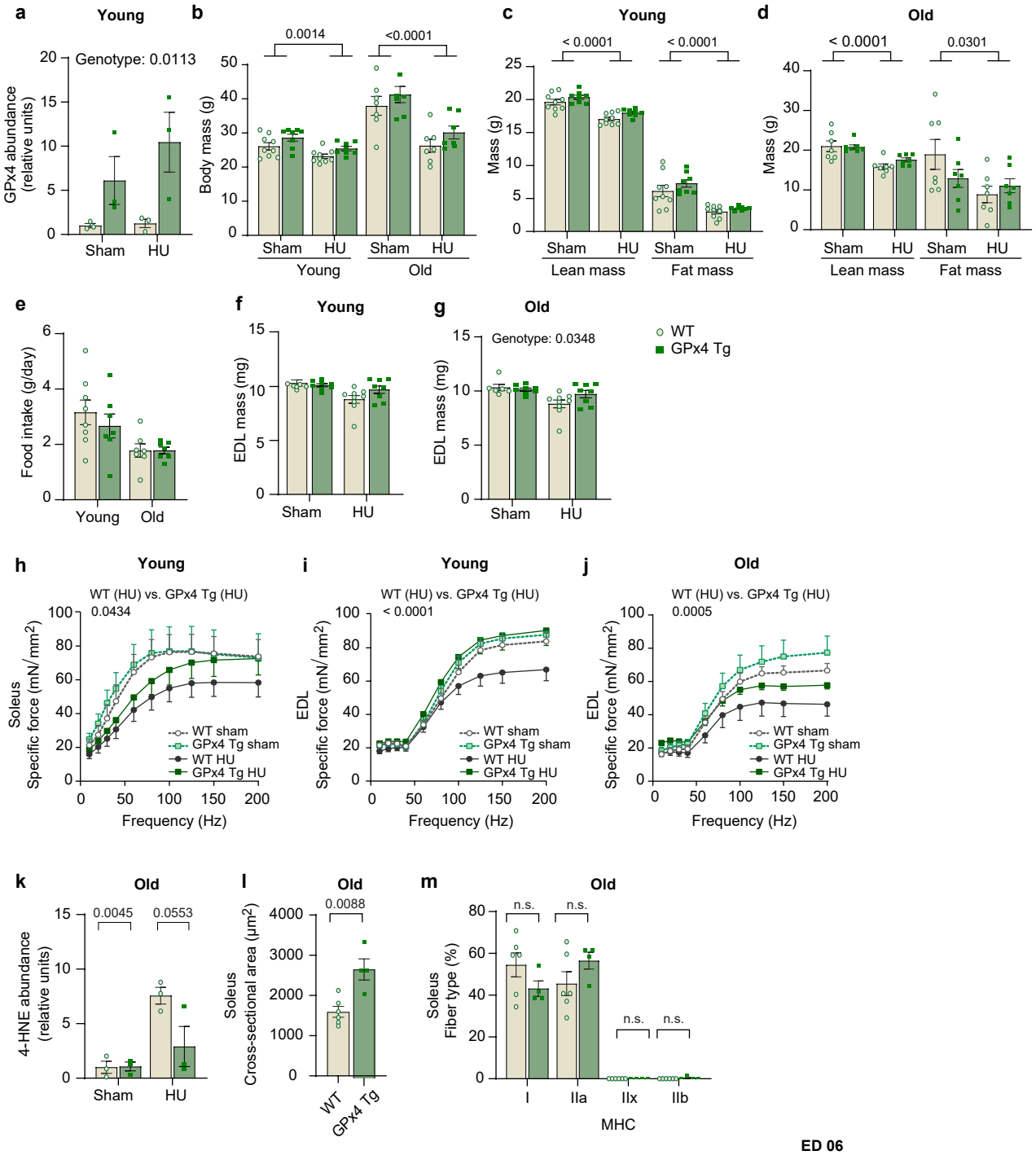
a
Young
Genotype: 0.0113
GPx4 abundance (relative units)
Sham
HU
b
0.0014
<0.0001
Body mass (g)
Sham
HU
Young
Old
c
Young
< 0.0001
< 0.0001
Mass (g)
Lean mass
Fat mass
d
Old
< 0.0001
0.0301
Mass (g)
Lean mass
Fat mass
e
Food intake (g/day)
Young
Old
f
Young
EDL mass (mg)
g
Old
Genotype: 0.0348
EDL mass (mg)
WT
GPx4 Tg
h
Young
WT (HU) vs. GPx4 Tg (HU)
0.0434
Soleus
Specific force (mN/mm²)
Frequency (Hz)
WT sham
GPx4 Tg sham
WT HU
GPx4 Tg HU
i
Young
WT (HU) vs. GPx4 Tg (HU)
< 0.0001
EDL
Specific force (mN/mm²)
Frequency (Hz)
j
Old
WT (HU) vs. GPx4 Tg (HU)
0.0005
EDL
Specific force (mN/mm²)
Frequency (Hz)
k
Old
0.0045
0.0553
4-HNE abundance (relative units)
Sham
HU
l
Old
0.0088
Soleus
Cross-sectional area (μm²)
WT
GPx4 Tg
m
Old
n.s.
n.s.
n.s.
n.s.
Soleus
Fiber type (%)
I
IIa
IIx
IIb
MHC

ED 06

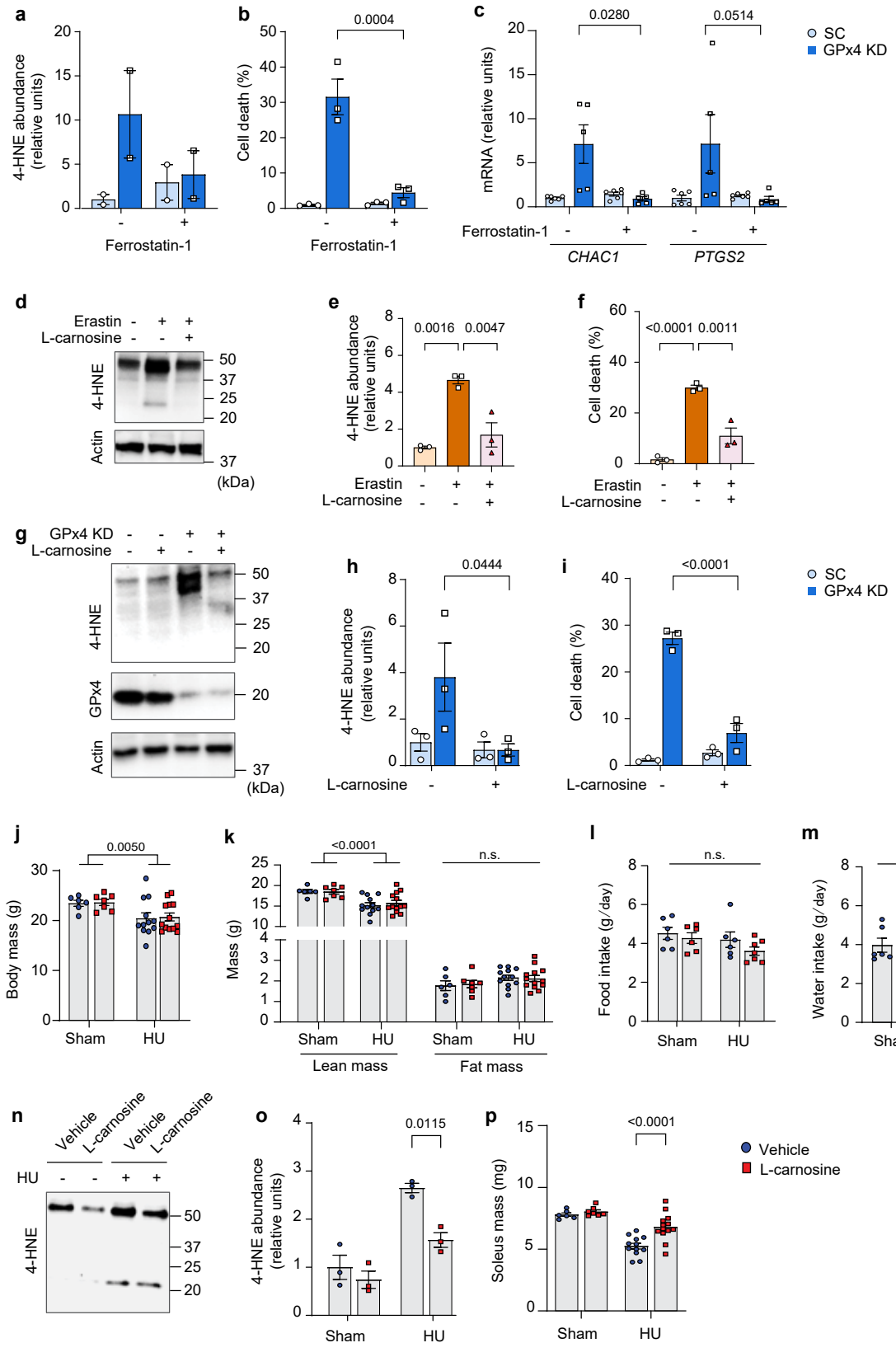
a
4-HNE abundance (relative units)
Ferrostatin-1
b
Cell death (%)
0.0004
Ferrostatin-1
c
mRNA (relative units)
0.0280
0.0514
SC
GPx4 KD
Ferrostatin-1
CHAC1
PTGS2
d
Erastin
L-carnosine
4-HNE
Actin
(kDa)
e
4-HNE abundance (relative units)
0.0016
0.0047
Erastin
L-carnosine
f
Cell death (%)
<0.0001
0.0011
Erastin
L-carnosine
g
GPx4 KD
L-carnosine
4-HNE
GPx4
Actin
(kDa)
h
4-HNE abundance (relative units)
0.0444
L-carnosine
i
Cell death (%)
<0.0001
L-carnosine
SC
GPx4 KD
j
Body mass (g)
0.0050
Sham
HU
k
Mass (g)
<0.0001
n.s.
Sham
HU
Lean mass
Fat mass
l
Food intake (g/day)
n.s.
Sham
HU
m
Water intake (g/day)
n.s.
Sham
HU
n
Vehicle
L-carnosine
Vehicle
L-carnosine
HU
4-HNE
o
4-HNE abundance (relative units)
0.0115
Sham
HU
p
Soleus mass (mg)
<0.0001
Sham
HU
Vehicle
L-carnosine

ED 07

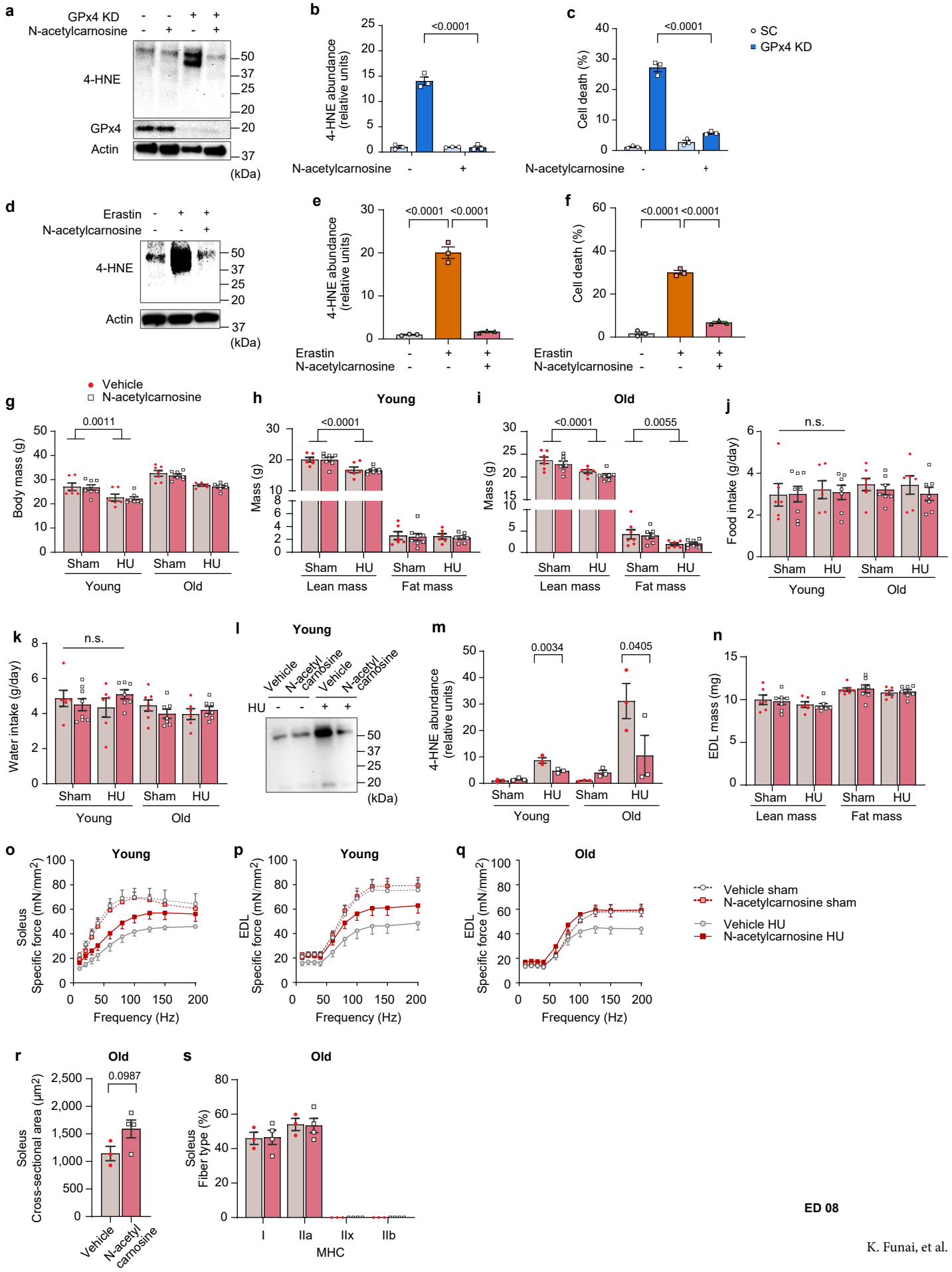

ED 08

K. Funai, et al.

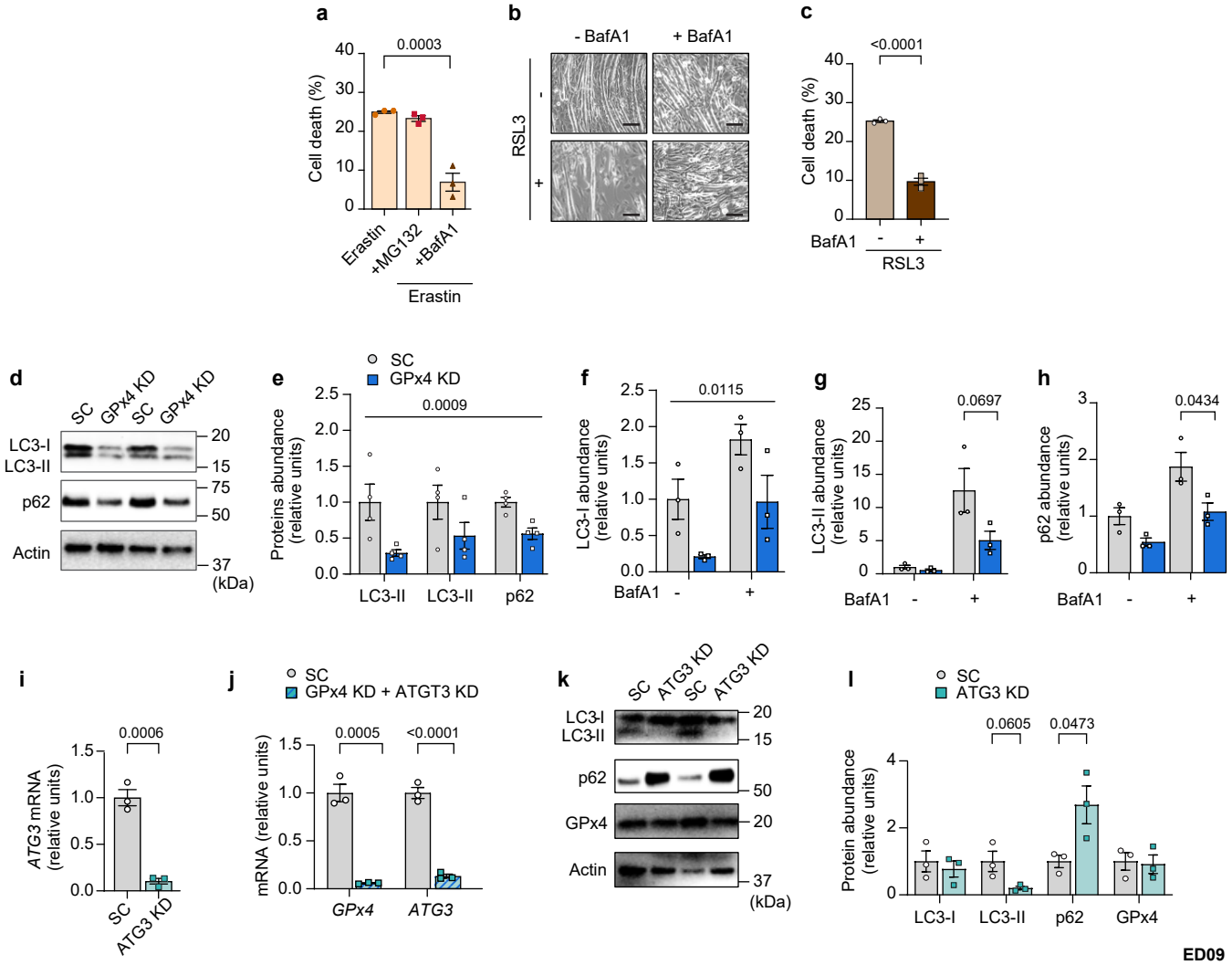
a
0.0003
Cell death (%)
Erastin
+MG132
+BafA1
Erastin
b
- BafA1
+ BafA1
RSL3
c
<0.0001
Cell death (%)
BafA1
RSL3
d
SC
GPx4 KD
SC
GPx4 KD
LC3-I
LC3-II
p62
Actin
(kDa)
e
SC
GPx4 KD
0.0009
Proteins abundance (relative units)
LC3-II
LC3-II
p62
f
0.0115
LC3-I abundance (relative units)
BafA1
g
0.0697
LC3-II abundance (relative units)
BafA1
h
0.0434
p62 abundance (relative units)
BafA1
i
0.0006
ATG3 mRNA (relative units)
SC
ATG3 KD
j
SC
GPx4 KD + ATGT3 KD
0.0005
<0.0001
mRNA (relative units)
GPx4
ATG3
k
SC
ATG3 KD
SC
ATG3 KD
LC3-I
LC3-II
p62
GPx4
Actin
(kDa)
l
SC
ATG3 KD
0.0605
0.0473
Protein abundance (relative units)
LC3-I
LC3-II
p62
GPx4

ED09

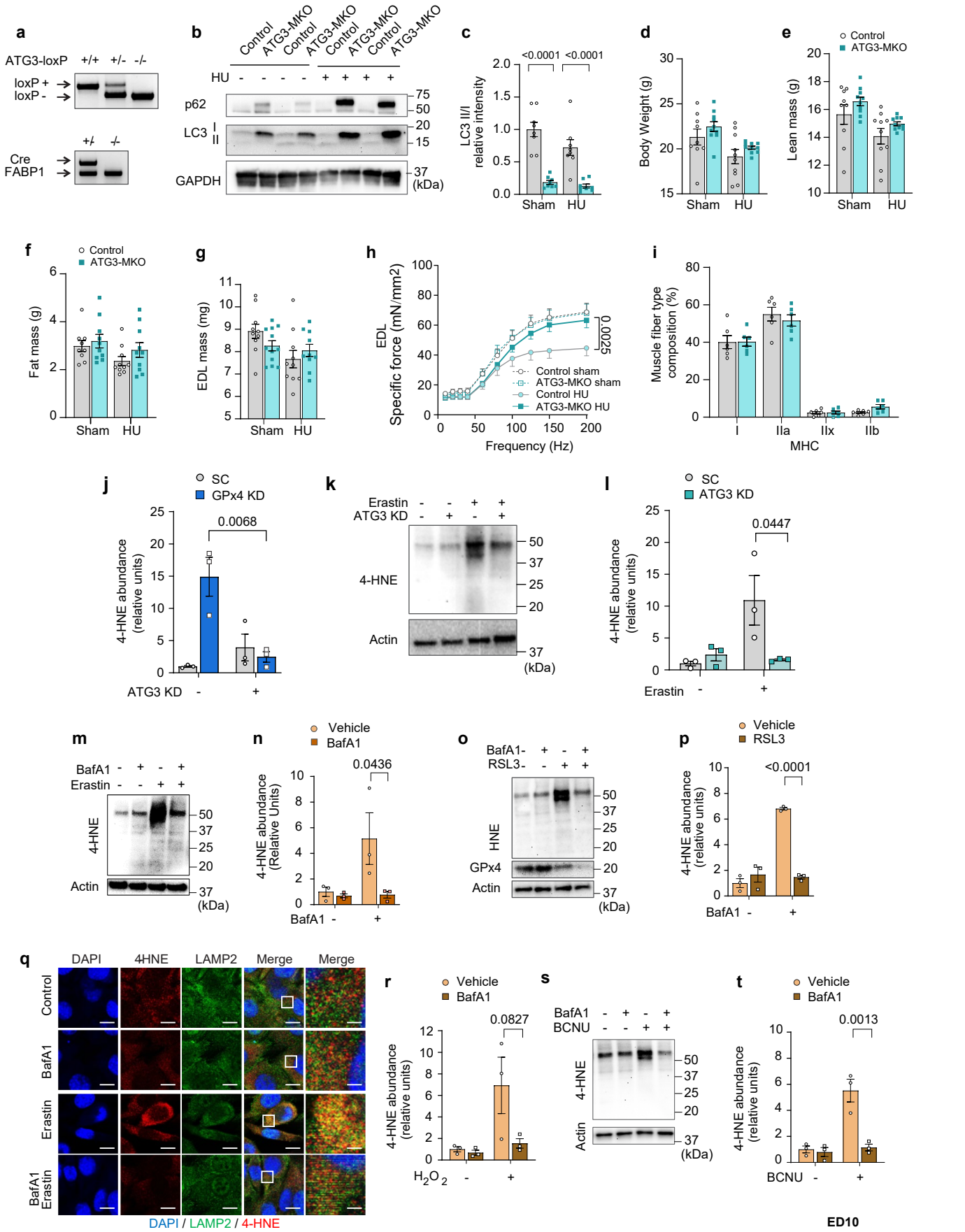

ED10

K. Funai, et al.